Title
MEASUREMENT OF IN-SITU STRESS IN ROCK USING NQR TECHNIQUES

Authors
Schempp, E.
Murdoch, J.
Klainer, S.M.

Publication Date
1982-04-01

Lawrence Berkeley Laboratory
UNIVERSITY OF CALIFORNIA

EARTH SCIENCES DIVISION

MEASUREMENT OF IN-SITU STRESS IN ROCK USING NQR TECHNIQUES

E. Schempp, J. Murdoch, and S.M. Klainer

April 1982

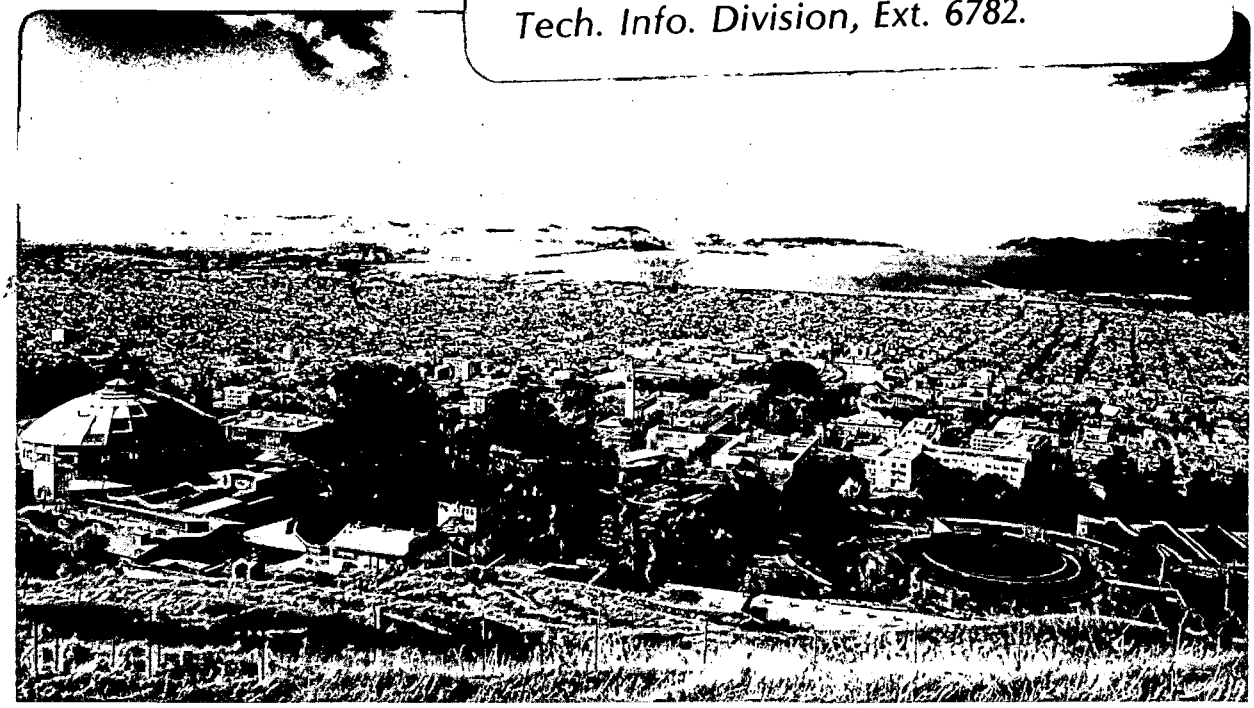

Prepared for the U.S. Department of Energy under Contract DE-AC03-76SF00098

DISCLAIMER

LBL-14411

MEASUREMENT OF IN-SITU STRESS IN ROCK USING NQR TECHNIQUES

E. Schempp, J. Murdoch, and S. M. Klainer

Earth Sciences Division
Lawrence Berkeley Laboratory
University of California
Berkeley, California 94720

April 1982

This work was supported by the Assistant Secretary for Nuclear Energy, Office of Waste Isolation of the U.S. Department of Energy under Contract DE-AC03-76SF00098. Funding for this project is administered by the Office of Nuclear Waste Isolation at Battelle Memorial Institute.

EXECUTIVE SUMMARY

A unique state-of the-art NQR spectrometer has been developed that has superior capabilities in terms of operation, data handling, and sensitivity especially suited for the low frequency region of alumino-silicate minerals which is essential for stress/strain measurements in granites, basalts, and some other rock. It incorporates a major technical advance: a new circuit design for bringing the after-pulse ringdown time to less than 20 micro-seconds, an order-of-magnitude improvement over pre-existing instruments. This is important because it extends the use of the NQR technique to wide spectral lines such as Al^{27}.

In addition, sophisticated experiments that use magnetic double resonance techniques to study the magnetic interactions in uniaxially stressed single crystals of NaCl and in polycrystalline salt are described. Although the quadrupole interaction of the chlorines could not be observed, it was shown that stress produces an easily measurable effect on the sodium NMR signal. Moreover, these experiments resulted in the surprising discovery of a "self-double-resonance" process which allows observation of the magnetic dipole-dipole interaction at almost zero field. Thus, a sensitive new technique for studying solids was discovered.

The lineshape calculations in stressed, randomly oriented polycrystal-line NaCl have paved the way for applying the NQR technique to rocks with aluminum-containing minerals. The experimental verification of the lineshape calculations is expected later this year. Mathematical considerations of the borehole perturbation indicate that NQR can be used effectively to obtain values of the pre-existing state of stress.

Finally, the successful observation of the quadrupole interaction in the mica muscovite, an important constituent in many granites, indicates that

nuclear quadrupole resonance lines can be observed in common rock-forming alumino-silicates. The frequency range is favorable, and for a preliminary study, the signal-to-noise ratio is reasonably good.

LBL anticipates no obstacles in the development of this project. Work to date has enhanced the probability of success in developing a new instrumental technique for the field measurement of stress in igneous rocks.

CONTENTS

LIST OF ILLUSTRATIONS

LIST OF ILLUSTRATIONS (Continued)

LIST OF ILLUSTRATIONS (Continued)

LIST OF ILLUSTRATIONS (Continued)

ACKNOWLEDGMENTS

The work described in this report was supported, until September 30, 1981, by the Office of Nuclear Waste Isolation, Battelle Memorial Institute, Columbus, Ohio. We wish to thank our program manager, Mr. Norman Henderson, for his valuable technical assistance, cooperation, and understanding.

We are also grateful to our colleagues at other institutions for their cooperation, assistance, and stimulating technical discussions. In particular, we wish to thank Dr. Robert A. Marino and co-workers at Hunter College, City University of New York, for their long-term interest in this work and for carrying out the measurements in mica. We also thank Dr. John Ragle and co-workers at the University of Massachusetts for making the measurements in salt, for fruitful discussions of double resonance, and for their kind invitation to one of the authors (E.S.) to participate in the experiments.

Several scientists at LBL also made essential contributions, expecially Dr. Branko Leskovar, Dr. C. C. Lo, and their co-workers in the Electronics Research and Development Group. Mr. Leif Hansen of the Mechanical Engineering Group is to be thanked for designing the stress jig for the salt measurments.

ABSTRACT

Recent advances have been made in the application of nuclear quadrupole resonance (NQR) to stress in underground rock. A high performance NQR spectrometer is near design completion and construction has begun. Double resonance experiments in stressed single crystals of NaCl were performed, the lineshape functions in stressed polycrystalline NaCl were calculated, and the first Al^{27} NQR spectra in minerals were observed by H^1-Al^{27} double resonance. Moreover, a new method has been developed for applying kilowatt pulses at low frequencies to a tuned tank circuit whilst keeping the ringdown time below 20 μsec.

Results to date indicate that initial projections for success in alumino-silicate minerals in rocks were well-founded. The lineshape calculations have shown how NQR can be applied to a randomly oriented polycrystalline material in the vicinity of a borehole to obtain the stress tensor. The method, however, appears not to be easily applicable to salt owing to the low value of the stress-induced quadrupolar coupling and the large dipole-dipole interaction of the sodiums. Quadrupolar coupling in muscovite (mica) was measured; at room temperature, $e^2qQ = 3.55$ MHz and $\eta = 0.265$ for the octrahedrally coordinated site.

1. INTRODUCTION

The measurement of stress in underground rocks is a difficult, but important, problem in mining engineering, because the structural stability of any excavation or mine depends critically on the stress distribution in the surrounding rocks and their capacity to bear the stress. In deep mines the pressure from the overburden can build up to hundreds of atmospheres.

But rock is far from homogeneous. Many rocks are aggregates of crystals or grains which are, in turn, polycrystalline. Moreover, most rock masses are crisscrossed by joints and cracks, and many are made up of multiple bedding planes. Finally, underground openings usually cut through rocks of different types, so that the mechanical properties of the material on one side of an irregular surface may be quite different from those in the rock on the other side.

All these features make it very difficult to calculate with accuracy the stress concentrations at a particular point. The stress must therefore be determined empirically. This, however, is also a formidable task; at present, no technique exists for making rapid, nondestructive measurements of the state of stress in rocks in-situ. The problem is especially acute for stress measurements in boreholes.

To this end, Lawrence Berkeley Laboratory is currently engaged in a research and development effort that focuses a new technology on the problem of stress measurement. That technology is nuclear quadrupole resonance (NQR) spectroscopy.

In the next several sections we summarize the first report in this series (Ref. 1), and in section 2 recent progress in the program is described.

1.1 NQR AND NUCLEAR MAGNETIC RESONANCE

Nuclear magnetic resonance (NMR) has been a well-developed tool in chemical and physical laboratories for more than 20 years. In NMR, use is made of the fact that the nuclei of many, but not all, atoms possess magnetic dipole moments and thus, like a compass needle in the earth's magnetic field, the nuclei tend to line up with the field lines in a large magnet. This tendency toward alignment can be detected using radiowaves of the proper frequency and duration. NMR figures importantly in the study of molecules and crystals because the nucleus senses small variations in its magnetic environment which arise from the magnetic fields produced by other nuclei and by electrons in the molecule or crystal. In effect, NMR uses the nucleus as a microscopic probe of its environment. This has proved a powerful technique for the study of solids and liquids.

Similarly, some nuclei also possess an electrical property which makes possible a special interaction with their electrical environment. That property is a nonspherical distribution of (positive) charge called the nuclear quadrupole moment, $\underline{Q}$. The more important atoms of geophysical interest whose nuclei have this characteristic include sodium, chlorine, aluminum, magnesium, and a low-abundance isotope of oxygen.

A quadrupolar nucleus interacts with electric charges situated in its neighborhood, more precisely, with the spatial derivatives of the electric fields produced by those charges. (The mathematical details can be found in Schempp, Hirschfeld, and Klainer.[1]) The electrical charges which contribute predominantly in this context are the valence electrons in covalent chemical bonds and ionic charges in the crystal. The quadrupolar interaction can be used to measure stress because strain deformation always occurs when a crystal is stressed. Strain entails geometrical changes in

the atomic positions in the lattice and thus in bond distances. Such changes invariably affect the electric field gradient and thus the degree of the quadrupolar interaction.

Since this interaction is detected in an NQR experiment by measuring the frequency at which radio waves are absorbed, small changes can be observed with high sensitivity. The derivatives of the electric field potential which determine the NQR frequency have the form

$$\frac{\partial^2 V}{\partial z^2} \alpha \frac{1}{r^3}$$

where V is the potential and r is the distance from the nucleus to the charge which produces the potential. A change in r of 0.01% due to strain may change the quadrupolar interaction by thousands of hertz.

A theoretical understanding of the (hydrostatic) pressure dependence of NQR frequencies is still in a relatively primitive state.[2,3] However, only the empirical observations are important in this discussion. Generally, $(\partial\nu/\partial P)_T$ is linear, but may be of either sign (ν is the frequency and P is the pressure); values up to 200 Hz/atm have been measured under hydrostatic pressure. It is important to realize that a simple relationship does not necessarily exist between the gross mechanical strain deformation in the crystal and the local distortion of the chemical bonds of a particular atom when the crystal is strained. Thus, strains on the order of 10^{-6} may produce much larger percentage changes in the NQR frequencies.

In the case of salt, no quadrupolar interaction exists in an unstressed crystal owing to the cubic site symmetry of the Na and Cl ions. However, when the crystal is strained non-isotropically, the cubic symmetry is lifted, and a quadrupolar interaction appears.

More sophisticated methods--known as nuclear double resonance techniques--can be applied when simple NMR or NQR experiments do not provide sufficient sensitivity.[1,4] Although many variations exist, fundamental to all double resonance experiments is the use of an easily detectable strong resonance signal to observe a weaker signal in another species. In aluminum minerals containing hydrogen (bound in water or hydroxyl groups), aluminum NQR transitions can be monitored by the changes they induce in the strong proton NMR signal. The Na NMR signal in stressed salt can be used similarly to observe the Cl quadrupolar interaction.

1.2 STRESS AND STRAIN

The electric field gradient (EFG) tensor V_{ij} is related to the stress tensor σ_{ij} by

$$V_{ij} = \sum_{kl} C_{ijkl} \sigma_{kl}$$

where the C_{ijkl}'s form a fourth rank tensor known as the gradient stress tensor. Values of the C's are measured in the laboratory and are different for each crystalline substance.

In cubic salt, the gradient stress tensor takes on a particularly simple form owing to the high symmetry, and values can be found in the literature. The resulting NQR frequencies were calculated[1] and are summarized in Table 1. The values in this table apply to single crystals of salt under conditions of uniaxial loading.

In aluminum minerals, unfortunately, relatively few Al^{27} NQR results have been published; therefore, the first priority is to detect the NQR lines in pure laboratory samples. Only then can the values of the gradient stress tensors be measured, again under laboratory conditions. It should be noted, however, that for noncubic systems, the gradient stress tensor has many more

TABLE 1. Calculated values for the NQR frequencies in uniaxially stressed NaCl at σ = 100 atm.

	Stress direction (NQR frequencies in kHz)		
	[100]	[110]	[111]
Na^{23}	2.8	2.1	1.8
Cl^{35}	2.3	5.2	6.0
Cl^{37}	1.8	4.1	4.7
Direction of z-principal axis	Parallel to σ	$[\bar{1}10]$, normal to σ for Na; parallel to σ for Cl	Parallel to σ
Asymmetry parameter	0	0.55 for Cl 0.30 for Na	0

nonvanishing components--up to 30 for the general triclinic case. Although it is not necessary to measure these elements individually, the empirical relationship between applied stress and the NQR spectrum of alumino-silicates will be more complicated than in the case of cubic systems like NaCl. Theoretical and laboratory procedures must be developed to handle these cases.

Nonetheless, aluminum NQR in minerals provides one great advantage over salt--the quadrupolar interaction occurs at significantly higher frequencies, typically 0.5 to 2.0 MHz, and is measurable in unstressed samples. Thus, the NQR lines can be readily observed, and the shifts in their position as a function of the magnitude and direction of the stress can be detected easily. Moreover, for noncubic systems the NQR shifts do not vanish in the case of hydrostatic pressure.

1.3 INSTRUMENTATION AND TECHNIQUES

NQR signals of the type described can be detected using either direct or indirect techniques. Indirect techniques are favored for situations where the sensitivity is expected to be low due to scant isotopic abundance or, as in NaCl, due to the very low frequencies involved. Nuclear double resonance (NDR) is one such indirect method.[4-7]

1.3.1 Nuclear Double Resonance

Nuclear double resonance (NDR) requires that the sample contain a nuclear species whose NMR or NQR signal is strong and easy to observe. For salt, a strong signal is available from the Na atoms when a relatively large magnetic field (a few thousand gauss) is applied. This signal is then observed at periodic intervals between which the sample is manipulated so that the sodiums interact with the chlorines. A change in the sodium resonance indicates that some energy exchange with the chlorine system has occurred, and thus the chlorine lines can be detected. This energy transfer between the two spin systems can be achieved several ways. One of the easier means is to turn the external magnetic field off (or, alternatively, remove the sample to a field-free region). As the sodium magnetization decays out of the field, the energy levels cross over the quadrupolar energy levels of the chlorines. If the chlorines are irradiated at their NQR frequency, the sodium signal is perturbed. The sample is then repeatedly cycled through a Cl irradiation pulse at stepped frequencies and a Na pulse at a fixed frequency; a decrease in the Na signal at the end of a particular cycle indicates detection of the chlorine signal. This procedure requires a magnetic field, which could be cumbersome in a field situation but offers the highest attainable sensitivity. It is virtually the only possible method for NaCl.

1.3.2. Pure NQR

In direct detection, it is necessary only to apply the proper radio frequencies to the sample and to detect the resulting nuclear signal. A variable, continuous wave (cw) oscillator can be used, but more commonly today a large short pulse is applied and the nuclear signal is observed in the time just after the pulse.[6,7] Such a signal is known as a free induction decay (FID). Pulse methods are well suited to aluminum because preliminary work has shown that signals are customarily observable in the 0.5 to 2 MHz range.

Pulse methods offer a number of advantages. Through Fourier tranform data processing, all the information available in a cw spectrometer is also obtained from the FID. In addition, pulse techniques are effective for a wider range of nuclear relaxation times, often provide higher sensitivity, reduce the time for data collection, offer more versatility for samples of varying characteristics, permit accurate determination of lineshapes, and make the search for new resonance lines much easier.

Instrumentation for both double resonance and pulsed NQR has been available for some time, although some modification of existing designs is required to optimize the signal-to-noise ratio and the operating convenience.

1.3.3 Field Systems

The most important requirement of the potential field instrument is the ability to measure stress in the vicinity of a borehole. Since a cylindrical hole perturbs the surrounding stress field, the NQR method must be able to observe the stress within approximately the first meter of the borehole wall; then, using the NQR measurements as a function of angle and depth, the three-dimensional stress state is determined. A detailed discussion of these

procedures is given in Schempp, Hirschfeld, and Klainer,[1] including an analysis of several kinds of directed antennas, the power requirements, and the data processing.

2. PROGRESS IN THE NQR STRESS MEASUREMENT PROGRAM

2.1 INSTRUMENTATION

A significant part of the FY'81 effort was the design of a sophisticated multiple purpose NQR spectrometer which incorporated the latest engineering concepts. The following design specifications are the culmination of many working sessions with consultants and LBL staff.

Frequency range	0.5 to 16 MHz initially, later to be extended to 72 MHz.
Maximum pulse height	3000 V_{pp} minimum, 4000 V_{pp} if possible.
Pulse length	1 to 1000 μsec.
Pulse repetition rate	DC to 10 kHz (up to 10% duty cycle).
Pulse sequences	$\pi/2$, π, with ±90° phase shift capability, plus Carr-Purcell, WAHUHA, Ostroff-Waugh, spin-locking, SORC, SLSE, cross-polarization sequences, and all other standard varieties; provision for adjustable programming of pulses.
Detection	Phase-sensitive quadrature outputs with fast A/D converter; dual channel FFT with on-line computer.
Pulse ringdown time	Better than 20 μsec to Johnson noise and better than 10 μsec if obtainable.
Receiver amplifier recovery time	10 μsec or better.
Pulse droop	Less than 1%.
Frequency stability	Better than 1 part in 10^8.

These exacting specifications were designed to hasten the development of a state-of-the-art instrument and to meet the wide variety of problems anticipated in geological samples--such as line widths ranging from a few hundred hertz to possibly a few tens of kilohertz, spin-lattice relaxation times ranging from milliseconds to minutes, and signal strengths ranging

from strong to the theoretical limits of detectability. In addition, the following design requirements were imposed:

- The instrument had to be usable in NMR work,
- The sample could be incorporated in a variable temperature head (at least 77-700°K),
- The instrument had to be adaptable to nuclear double resonance experiments, and
- Provision could be made at a later date for automatic frequency scans.

The primary purpose of the instrument was to detect and measure the NQR line frequencies and relaxation times of Al^{27} nuclei in rock and clay minerals. As envisioned, the spectrometer would at some stage be used for investigating S^{33}, O^{17}, Ca^{43}, Mn^{55}, Ti^{47}, Mg^{25}, and other important crustal elements.

Modular-type construction was selected as the better means of achieving the specifications and high sensitivity. Separate component modules provide for flexibility and versatility and also allow for higher isolation. Reducing the chances of interfering leakage signals, which would diminish the noise figures of the high gain receiver circuits, is essential to assure high detection sensitivity. This is particularly important when very high power rf signals are in close proximity to sensitive receivers and gating circuits. In addition, modules permit relatively easy modification and future upgrading of the system.

A second major decision was to build a spectrometer around heterodyning principles. This makes some timing and gating procedures easier, and gives much more accurate control of the signal phase, which is highly desirable in an FFT unit. Heterodyning also contributes to maintaining very high sensitivity.

The overall design was strongly influenced by Dr. Klainer's experience with a previous instrument built by Block Engineering.[8] This made it possible to avoid some of the mistakes and problems then encountered.[9] The overall design responsibility was given to Dr. B. Leskovar and co-workers, of the Electronics Research and Development Group at LBL, because of their considerable experience in designing and building pulsed NMR equipment. A block diagram of the final spectrometer design is shown in Fig. 1.

The ringdown time was expected to be the most difficult specification to achieve. Following a high power pulse delivered to a tuned circuit, the oscillating energy does not dissipate instantly; rather the oscillations die out exponentially over a period of up to several hundred microseconds. This problem is particularly acute at low frequencies. The ringdown time of the previous instrument is 150-200 μsec.[9]

Ringdown time is different from recovery time. The latter refers to the recovery from saturation due to overloading of the rf amplifier/receiver circuits which occurs when an amplifier designed to amplify at the microvolt range is overdriven by the high voltage pulse. (In fact, the receiver must be protected from this pulse by shunting and gating circuits.) Long recovery and ringdown times are disadvantageous because no signal from the sample can be detected during these periods. If the complete free induction decay cannot be recorded, important information is lost.[10] This is particularly serious in the case of lines with large natural linewidth because such lines have very short FID's (the FID is the Fourier transform of the absorption line). A line 10 kHz wide will have a FID which lasts only ~ 100 μsec. Thus, a wide line will not be observed at all if the recovery and ringdown times are long.

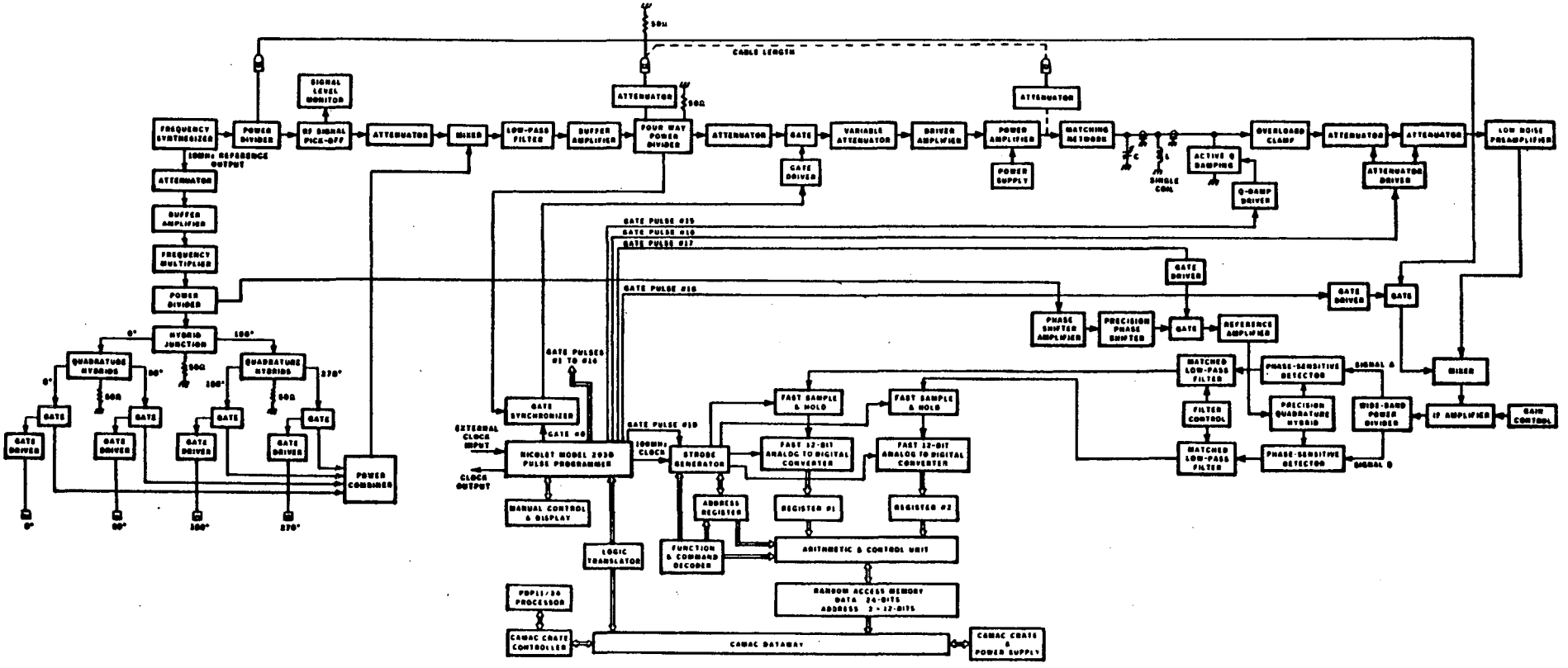

Figure 1. Block diagram of the final spectrometer design.

With good circuit design and modern components, recovery time can be kept in the several microsecond region. Therefore, the limiting factor is the ringdown time, and this was singled out for the major development effort in the first year of the construction program. The basic idea in shortening the ringdown time is to find a scheme by means of which the energy contained in the coil can be dumped or dissipated, i.e., the nominal coil Q of 10 to 100 must be quickly converted at the end of the pulse to a Q of much less than 1 for a short period, and the high Q state must be quickly recovered while listening to the nuclear signals. This technique is called "dequeing" or "Q-spoiling." Dequeing is difficult in this situation because of the high rf voltages which cannot be tolerated by usual switching components, diodes and transistors. The dequeing scheme also must not introduce new time constants and circuit loading which would reduce the signal strength.

2.1.1 Transmitter and Dequeing Circuit Design

Since the signal generating part of the transmitter is fairly well defined, emphasis was put on developing the final stage of the transmitter, the dequeing scheme, and the control circuit for attenuating the high power signal during transmitting without producing significant transients which would saturate the high gain preamplifier.

A prototype final stage was constructed to study the recovery time and ringdown time of the final amplifier. An Eimac 8877 triode was used in a grounded grid configuration with a single coil and single capacitor tank circuit. The sample coil is part of the tank circuit; the arrangement allows the high power transmitting signal and the extremely low level sample-produced signal to be dealt with effectively, while at the same time keeping the tuning, through one octave of bandwidth, to a single control.

Initially, a decoupling capacitor was used to isolate the DC plate voltage from the sample. A prototype was built and measured to determine if the scheme was feasible; however, the recovery time of the decoupling capacitor was not acceptable. After numerous measurements and consideration of alternatives, a second design was built. This time the triode was grounded through the tank circuit, eliminating the need for a decoupling capacitor. The final stage operated effectively as a grounded grid amplifier with a grounded plate configuration.

The dequeing problem required that a number of different devices be screened and tested for suitability, such as microwave diodes, planar triodes, and hex fets. One microwave planar diode was tried in conjunction with the final amplifier stage, but did not serve the dequeing process well enough because of higher-than-desired resistance during full conduction. High power hex fets initially appeared very promising, but such devices (at their present state of development) are not compatible with this application due to their very high zero-bias shunt capacitance (more then 1000 pf).

Finally, the decision was made to use another Eimac 8877 triode operating in a grounded cathode configuration as the dequeing "crowbar." At the end of the transmitting cycle, this triode is turned on by a positive grid pulse so hard that it essentially looks like a short circuit to the tank circuit, thus dissipating most of the energy stored in the tank. No other device could match the ruggedness and other characteristics of the Eimac 8877 triode for this application. The results were encouraging enough to consider the scheme as the tentative final design for this stage. Indeed, ringdown time was brought below 20 μsec for pulses at 6 MHz, which contrasts markedly with the 150 μsec obtainable with the best available instruments heretofore.[8,9]

The final stage was never operated at maximum power level mainly because proper components were not available and the required driving power could not be provided by existing equipment.

Although the final amplifier stage looks promising, the next big hurdle is to provide an extremely low-transient-producing electronic attenuator to protect the preamplifier input stages from the direct transmitter signal. Approximately 180 dB of attenuation is required to reduce the transmitting signal to a level acceptable to the preamplifier. At the same time this electronic attenuator must turn on and off at high speed without producing any transient which may saturate the preamplifier.

Due to the restricted funds available, both time and component procurement were limited; hence, the development of the electronic attenuator and preamplifier is still in an early state. More effort is required to obtain proper attenuator and preamplifier performance. To date, the operating power is limited to 100-150 watts; recovery and ringdown time to the linear region of the preamplifier is approximately 7 μsec whereas ringdown time to the noise floor is about 14 μsec. A block diagram of the transmitter-sample coil stage is shown in Fig. 2. This work was largely performed by Dr. C. C. Lo of the Electronics Engineering Group at LBL.

2.1.2 Transmitter-Sample Probe Circuits

Shielding is an important circuit design consideration. Since 180 dB of attenuation is required, a Faraday cage is not sufficient. Heavy-duty filters between the transmitter and its power supply are required to prevent rf transmission in unwanted directions. To this end, the project benefits from Dr. Leskovar's considerable experience in shielding high power transmitters. The transmitter will operate off a regulated power supply, which

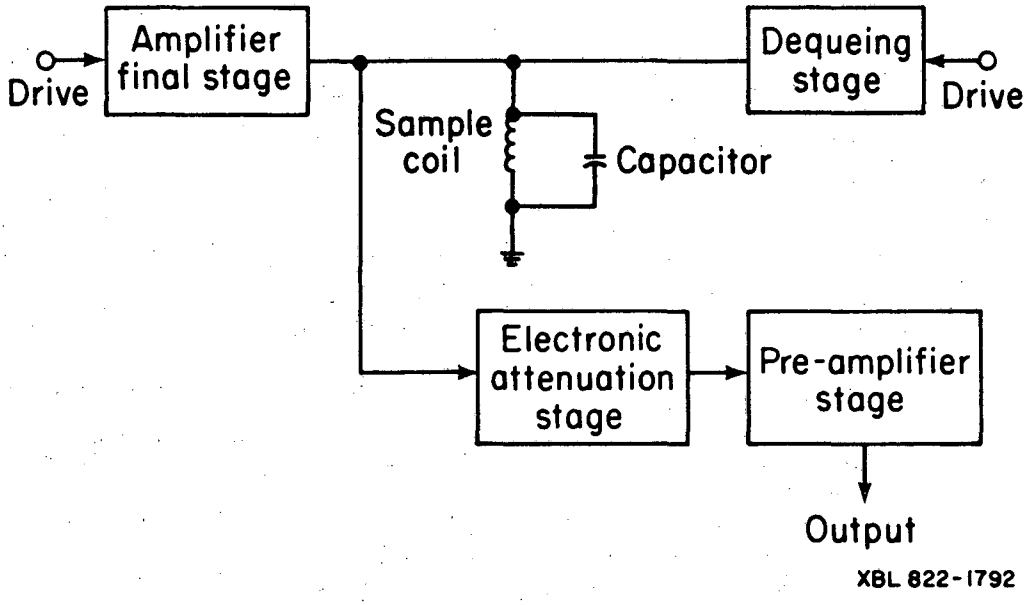

Figure 2. Transmitter-sample coil stage.

helps to achieve isolation. The 2 kW minimum pulse power will provide short pulses with less than 2% sag.

The output stage has been breadboarded but can be tested at full power levels only when a proper power supply is available. The power supply may be purchased commercially. The transmitter section can thus be completed fairly soon.

2.1.3 Preamplifier and Receiver

The special features in the design of the preamplifier and receiver circuits are low-crosstalk attenuators for the preamplifier, matched (to better than 2%) low-pass filters in the receiver, an IF amplifier with a 90 dB gain at 60 MHz with three layers of shielding, and careful attention to the filtering on all supply lines. The receiver will be constructed in a Nuclear Instruments Module (NIM) rack.

An important receiver design consideration is to achieve a wide dynamic range--performance is projected to provide better than 70 dB with less than 1 dB distortion. The receiver output is in two channels in quadrature so that no phase information is lost.[11] The two channels will be very carefully matched in amplitude (gain) to 1-5% accuracy and in phase to 2-10% accuracy. This requires very careful selection of all components.

The receiver is perhaps the most delicate part of the instrument and must be provided with exceptional shielding to make it essentially immune to rf interference, including that from the system's own transmitter. In addition, in order to isolate the receiver from the transmitter and timing signals, it must be furnished with ultrafast and ultralinear gates to switch the receiver on and off at the right times. This must be accomplished in such a way that the receiver dead-time is not appreciably lengthened and stray transients are not introduced.

The analog section of the receiver is presently under construction. Almost all electronic parts have been purchased and received, and the fabrication of the boxes and custom-made shielding is about half complete. The IF amplifier has been built, shielded, and tested. The matched lowpass filters have been completed except for the shielding. The power supplies have also been purchased, and the shielding and filtering are almost finished.

Overall, it is expected that the receiver can be completed quickly. The key problems will come during testing with the inevitable modifications to ensure good shielding, matching, stability, and linearity. However, one problem has been the unavailability of several components used successfully in previous receivers in NMR research. Therefore, construction has had to be delayed while substitute components and sources have been evaluated.

2.1.4 Digital Conversion and Data Processing

The analog signal from the receiver must be converted to a digital signal which can be handled by a computer. This is necessary first to increase the information gained by employing Fourier transform techniques[11] and second because the rate of data flow requires some form of temporary storage. Also the signal-to-noise ratio can be greatly enhanced by using signal-averaging techniques, which are best handled digitally.

The spectrometer requires a very fast A/D converter, operating at a 1 MHz rate. Following A/D conversion, the digitized signal will be held in sample-and-hold storage and then read into the main computer at a slower rate. After considering several options, including the commercially available Nicolet signal averager and the Biomation transient recorder, LBL decided to build its own averager and achieve either superior performance or lower cost.

The final data processing stage will make use of a DEC PDP-10 minicomputer. This choice was dictated largely by availability and familarity. Output capabilities will include chart recorders and video display screens.

Another important part of the digital circuitry is the pulse programmer. This unit provides the vital timing and gating signals which control the pulses, their phase, and all subsequent operation of the transmitter, receiver, and digitizing circuitry. After ample consideration, the present plan is to build this unit at LBL because commercial pulse programmers are either inadequate or they cannot be purchased separately, e.g., from Nicolet.

2.1.5. Instrument Setup and Location

The laboratory instrument will be placed in a shielded room, i.e., a well-constructed Faraday cage. This is necessary both to prevent outside rf from interfering with the NQR signal observations and to prevent the high power rf pulses from causing interference in nearby experiments in other laboratories and in commercial radio reception. (It should be noted that in the field, the rock surrounding a borehole provides a natural shield.) The spectrometer electronics and sample head will be contained in the shielded room. The computer will be outside the room; communication between the two will be via optical couplers.

2.1.6 Program Plans

When funds become available the following program can be met:

- Complete the transmitter and test the shielding.
- Develop and construct the preamplifier.
- Complete the construction of the receiver.
- Build the digital section of the output.

At this level, the spectrometer, although not complete, can nonetheless be used for some experimental work, assuming that a computer can be borrowed, and that part of the low-power rf front end can be simulated using available equipment such as frequency synthesizers and general purpose laboratory pulse generators. Ultimately, it will be necessary to provide phase-shifting networks, gating, and more versatile pulse programming capability. Total computer control, including automatic sweep and search, is also considered desirable in the long run.

With adequate funding, the spectrometer could be completed in about one year.

2.2 THEORY AND METHODOLOGY

Two requirements must be met when using the physics of the nuclear quadrupolar interaction to measure stress: NQR lines in rock minerals must be detectable, and these lines must contain all the information needed to extract values for the in-situ stress components. The first requirement has been met for selected Al^{27} samples.

The basic theory of NQR has been given,[1] wherein V_{ij}, the electric field gradient (EFG) tensor experienced by a given nucleus, is linearly related to the stress tensor σ_{ij} by

$$V_{ij} = \sum_{k=1}^{3} \sum_{l=1}^{3} C_{ijkl}\sigma_{kl} \qquad [1]$$

where $\underline{C}$ is the fourth-rank "gradient elastic tensor." The number of unique, non-zero elements of $\underline{C}$ depends on the site symmetry of the nucleus in the crystal. For the general triclinic case, there are 36 independent elements in a fourth-rank tensor which relates two symmetric second-rank tensors.[12]

However, the requirement that V be traceless[1] introduces a constraint on C:

$$\sum_j C_{jjk\ell} = 0, \qquad [2]$$

These six equations reduce the maximum number of independent elements to 30.

Obviously, a complete laboratory determination of all 30 values would still be formidable. In fact, the few measurements to date of the gradient elastic tensor have been performed on cubic crystals with only two independent components of $\underline{C}$. Fortunately, such an involved analysis is not necessary to relate the lineshape in a random polycrystalline sample to the applied stress.

The problem thus has two parts: the calculation of the "powder pattern" lineshapes in a randomly oriented polycrystalline sample under stress, and the modification of these lineshape patterns due to the borehole perturbation.

In the absence of a borehole, the unperturbed stress in a region can be expressed as a symmetric second-rank Cartesian tensor. Therefore, the stress tensor can be completely described in terms of three principal values and three angles giving the orientation of the principal axes. Because a random polycrystalline material knows no special direction in space, its NQR spectral frequencies will not be a function of the principal axes. That such material acts as a "principal value detector" is a substantial simplication.

The analysis is simplified by introducing the following quantities:

$$\bar{\sigma} = \frac{1}{3}(\sigma_{ii} + \sigma_{jj} + \sigma_{kk}) = \text{the hydrostatic stress.} \qquad [3]$$

If the axes are labelled such that

$$|\sigma ii - \bar{\sigma}| \geq |\sigma jj - \bar{\sigma}| \geq |\sigma kk - \bar{\sigma}|, \qquad [4]$$

we define the "stress anisotropy" $\delta(\sigma)$

$$\delta(\sigma) = |\sigma_{ii} - \bar{\sigma}|, \qquad [5]$$

where $\delta(\sigma)$ represents the largest deviation from the average, hydrostatic, stress. Similarly the "stress asymmetry" $\varepsilon(\sigma)$ is defined by

$$\varepsilon(\sigma) = \frac{\sigma_{jj} - \sigma_{kk}}{\delta(\sigma)}. \qquad [6]$$

From the definition, it is obvious that

$$0 \leq \varepsilon(\sigma) \leq 1, \qquad [7]$$

and that when $\varepsilon(\sigma) = 0$, the stress is uniaxial. The three quantities $\bar{\sigma}$, δ, and ε wholly determine the magnitudes of the three principal stress values, but can be more easily related to the resulting NQR lineshape. Their effects on the NQR lineshapes can be briefly summarized as follows:

- A purely hydrostatic stress ($\bar{\sigma} \neq 0$, $\delta = \varepsilon = 0$) will in general cause NQR lines to shift, usually to higher frequencies. Such stress will <u>not</u>, however, cause line broadening. The EFG parameters eq and η are functions of $\bar{\sigma}$; changes in both have been measured in the laboratory using a fluid-filled pressure cell. Numerous accounts in the literature describe experimental determinations of the pressure dependence of NQR transitions.[2] Harley <u>et al.</u> have performed such measurements on spodumene,[14] a lithium alumino-silicate, and Belitskiy <u>et al.</u> have investigated edingtonite,[15] $BaAl_2Si_3O_{10}\cdot 4H_2O$. However, in the case of cubic crystals (e.g., salt) where the quadrupole interaction vanishes by symmetry in the absence of stress, the quadrupole interaction will also be zero under hydrostatic pressure.[1]

- A stress anisotropy $\delta(\sigma)$ (which is often greater in magnitude than $\bar{\sigma}$) will cause both a shift in the transition frequencies and line broadening. The relationship between lineshape and δ can be studied by applying uniaxial stress to a single crystal sample in the laboratory.

- The stress asymmetry $\epsilon(\sigma)$ will cause additional line-broadening and frequency shifts, although perhaps to a lesser extent than caused by $\delta(\sigma)$. No experiments have been performed to date in which a triaxial stress has been applied to a quadrupolar sample.

The general problem of calculating NQR powder lineshapes is discussed in detail in the Appendix. Lineshapes for sodium chloride under uniaxial stress and varying experimental conditions have been computed.

In the immediate vicinity of a borehole, the stress pattern is significantly modified. However, a given set of unperturbed principal stresses gives rise to a characteristic borehole stress pattern, and this pattern can be mapped by NQR. A useful simplification results if it is assumed that one of the unperturbed principal stress axes is "vertical." This is often a reasonable assumption because at depth the lithostatic overpressure is downward.

With the assumption that one value of the stress is vertical and parallel to the borehole axis, only one azimuthal angle ϕ is needed to describe the orientation of the horizontal axes. Thus there are only four parameters to be determined: σ_{xx}, σ_{yy}, σ_{zz}, and ϕ. The borehole perturbation is then reduced to a two-dimensional problem with a well-known analytic solution.[16] A computer drawing which simulates the borehole stress for one set of conditions is shown in Fig. 3.

LBL has calculated the stress parameters $\bar{\sigma}$, $\delta(\sigma)$, and $\epsilon(\sigma)$ in a borehole region using a computer for each of the three types of stress distributions analyzed by Jamison and Cook:[17]

- Normal faulting, the vertical stress is the maximum principal stress;
- Thrust faulting, the vertical stress is the minimum principal stress;
- Strike-slip faulting, the vertical stress is the intermediate principal stress.

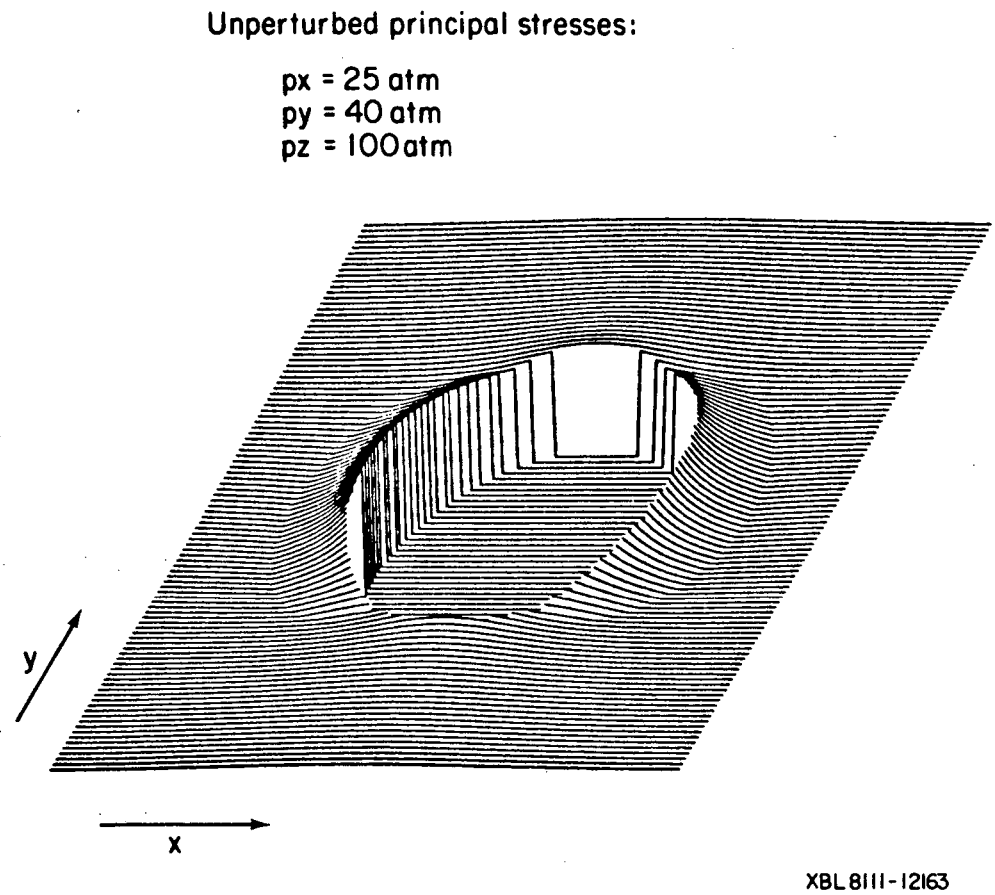

Figure 3. Stress anisotropy around a borehole. The maximum value of $\delta(\sigma)$ on this plot is 65 atm. The unperturbed value far from the borehole is 45 atm.

In general, the unperturbed stress tensor will be determined by comparison of an NQR map of principal stress values with borehole patterns calculated for various unperturbed stresses. This is possible because each set of unperturbed stresses results in a unique and characteristic borehole stress pattern. By varying coil orientation, magnetic field strength, etc., the NQR spectra can be taken at varying directions and distances into the rock from the borehole. When Al^{27} is the target nucleus, each NQR spectrum consists of three transitions,[13] each having an associated lineshape and average frequency. NQR spectra can be generated in the laboratory for known values of the hydrostatic stress, uniaxial stress, and, possibly, triaxial stress in order to obtain the necessary empirical calibrations.

With all of this data available, a computer can be programmed to do the following steps to obtain a reconstruction:

- Input the NQR lineshapes from field measurements as a function of angle and distance from the borehole wall;
- Determine the stress parameters $\bar{\sigma}$, $\delta(\sigma)$, and, possibly, $\varepsilon(\sigma)$ at these various locations, by comparing with the laboratory data;
- Calculate the borehole stress pattern;
- Output the unperturbed stresses.

2.3 EXPERIMENTAL STUDIES ON MINERALS

In order to make an experimental test of the concepts during the period when LBL's NQR instrument was being constructed, LBL supported research work at two universities in 1981. The results of the investigations are given in this section.

2.3.1 Aluminum Minerals

Since granite is a rock with a number of virtues as a possible repository site, it was decided to concentrate on the minerals found in typical granites:

Quartz	20-60%, no quadrupolar nuclei
Feldspars	20-75%, Al^{27}, Na^{23}, and K^{39} present
Micas and hornblendes	5-20%, Al^{27}, K^{39}, some Na^{23} and Mg^{25}, plus H^{1}.

The research work was performed by Dr. R. Marino and Dr. S. Sengupta of the Physics Department, Hunter College, CUNY, New York.

The first efforts were devoted to setting up a double resonance spectrometer for H^{1}-Al^{27} double resonance. Muscovite (mica) was chosen for the initial sample. Double resonance provides greatly enhanced sensitivity in the detection of NQR lines when the transition frequencies are low and the concentration of quadrupolar nuclei per unit volume is small.

2.3.1.1 Theory. Two different double resonance techniques can be applied to the H^{1}-Al^{27} system in a polycrystalline specimen. One is double resonance in the laboratory frame (DRLF), first introduced by Slusher and Hahn.[18] In this method, the sample containing two spin systems, A and B (H^{1} with I = 1/2 and Al^{27} with I = 5/2, in this case), is first polarized in a large DC magnetic field (10 kgauss) for a time sufficient for both sets of spins to return to equilibrium with the lattice temperature (Fig. 4). The specimen is then bodily removed to a region of zero magnetic field, where for the Al^{27} nuclei there are three doubly-degenerate energy levels in the presence of an EFG (Fig. 5). During the transit out of the magnetic field, the A spins are adiabatically demagnetized (that is, the entropy and the spin populations do not change), but the Zeeman splitting of the A-spin energy

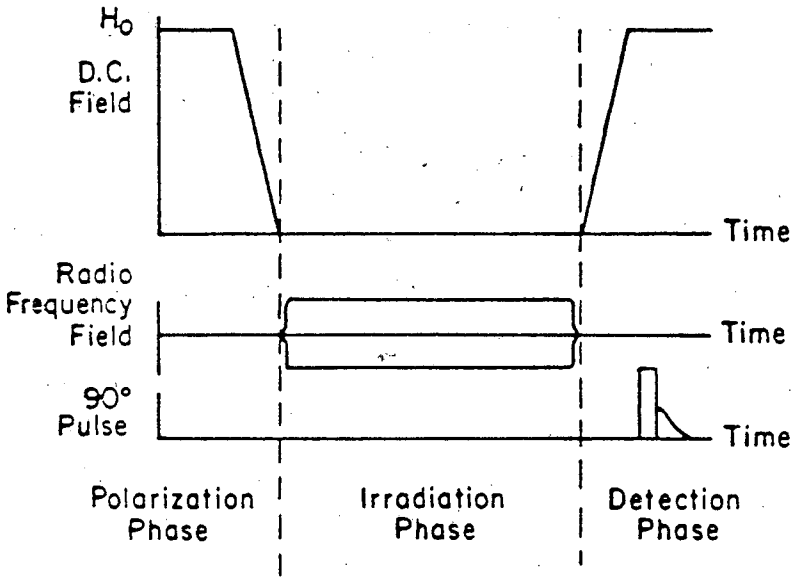

Figure 4. Timing diagram for nuclear double resonance experiment.

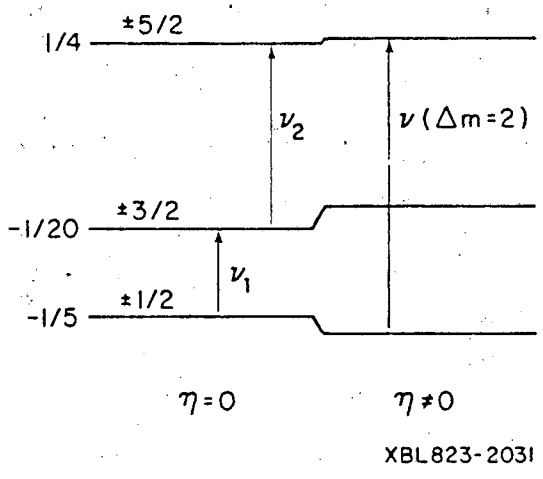

Figure 5. The quadrupole energy levels (in units of e^2qQ) and transition frequencies ν for a spin 5/2 nucleus such as Al^{27}.

levels collapses, becoming coincident successively with the three B-spin energy levels. This partially polarizes the B spins as they reach the zero-applied-field region. The transit time is on the order of 1 sec.

A radio frequency field of frequency $\underline{\omega_B}$ and amplitude $\underline{H_{1B}}$ is now applied. If this field $2\underline{H_{1B}}\cos \underline{\omega_B t}$ matches the energy splitting of the B-spin system, power will be resonantly absorbed and the B-spin population will change. Furthermore, if

$$\gamma_B H_{1B} = \gamma_A H_L \qquad [8]$$

where γ_A and γ_B are the magnetogyric ratios of the two nuclei and H_L is the local magnetic field at the A-spin site, then the two spin systems are brought into thermal contact if there is dipolar coupling between them (i.e., if the B-spins contribute to H_L). Power can thus be transferred to the A-spin system through the B-spins. This has the effect of increasing the A-spin system entropy, which results in a decrease in the subsequent (high field) A-spin magnetization.

At the end of this irradiation period the sample is returned to the large magnetic field where the A-spin magnetization is measured. During this return transit, three level crossings again occur, in inverse order to the polarization phase, and further A-spin polarization can be lost to the B-spins. The remaining A-spin (H^1) magnetization is monitored by applying a 90° pulse which stimulates a free induction decay (FID).

The second method is called double resonance with spin mixing by level crossing (DRLC), which was first used by Koo.[19] The procedure is basically the same, but the coupling between the A and B spins is established during the second set of level crossings which occur when the sample is remagnetized during the return transit. It is important to note that the sensitivity of both methods is independent of the frequency of the transition to be detected.

The total change in the final proton magnetization is also largely independent of $T_{1p}(0)$, the zero-field spin-lattice relaxation time of the protons.[20] If $T_{1p}(0)$ is large compared to the irradiation time, the proton system "remembers" the energy directly transferred to it during the irradiation. On the other hand, when $T_{1p}(0)$ is short, the protons, in essence, maintain thermal equilibrium with the lattice so that the effect of energy transfer during the irradiation cycle is lost. The proton magnetization is partially restored by the B spins during the second level crossing, but the extent of remagnetization depends on the magnetization remaining in the B system after irradiation.

2.3.1.2 Experimental Apparatus. A block diagram of the double resonance apparatus is shown in Fig. 6. An Arenberg high power rf oscillator is used to generate the 90° pulses for the proton system. Typical pulse widths are about 5 μsec at 41 MHz. The signals are amplified by a Matec broadband preamplifier and receiver, detected, and integrated with a boxcar integrator built at Hunter College. A gate width which covers about 25% of the FID intensity was found to give best results.

A programmable frequency synthesizer is connected to the second rf channel at coil B through an ENI power amplifier. This arrangement provides the few gauss of rf field sufficient to observe a change in the proton magnetization when the Al^{27} spins are irradiated.

2.3.1.3 Results in Mica. The region from 0.2 to 2.0 MHz was scanned at room temperature by repeatedly monitoring the proton FID as the B-channel frequency was stepped after each cycle. A cycle time of 60 seconds and an irradiation time of 6 seconds were used. The transit time from the DC magnetic field to zero field, a distance of about 20 inches, was about 1 sec.

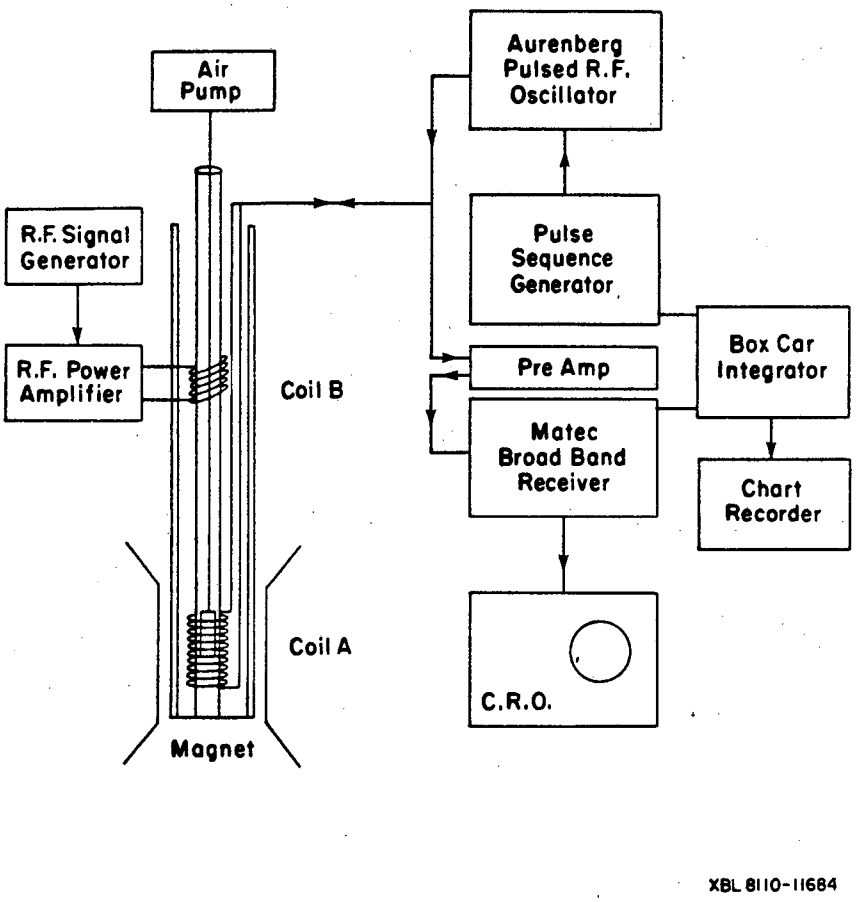

Figure 6. Nuclear double resonance spectrometer.

Mica exists in the form of thin sheets. These were broken and ground roughly in a mortar and packed into a Teflon sample tube a little less than 0.5 inch in diameter and about 0.7 inch long.

The frequency scan yielded three clearly defined signals which are shown in Fig. 7. The three lines are centered at 1624.5 kHz, 1052.0 kHz, and 572.5 kHz, with linewidths of about 1.8 kHz. Since the highest frequency is the sum of the other two, it is clear that all three lines belong to the same aluminum site. Using standard tables of the eigenvalues,[21] the quadrupole coupling constant e^2qQ and asymmetry parameter η can be calculated. The results are shown in Table 2.

TABLE 2. NQR data for the octahedral Al site in muscovite at room temperature.

Transition	Frequency (kHz)	e^2qQ (kHz)	η
$\pm 3/2 \rightarrow \pm 1/2$	572.5		
$\pm 5/2 \rightarrow \pm 3/2$	1052.0	3554.8	0.2646
$\pm 5/2 \rightarrow \pm 1/2$	1624.5		

Muscovite has the chemical composition $KAl_2(AlSi_3O_{10})(OH)_2$ and consists of layers of aluminate and silicate polyhedra. The crystal structure was determined by X-ray methods many years ago,[22] and the structure has been refined using electron diffraction techniques.[23] The unit cell is monoclinic, space group C2/c, and there are four formula units per unit cell. The crystal structure shows that there are three crystallographically distinct aluminum sites: two have aluminum tetrahedrally coordinated to four bridging oxygen atoms, and one has aluminum octahedrally coordinated to four bridging oxygens and two hydroxyl groups. Since the double resonance technique is sometimes more effective when the two atoms are geometrically close, the lines shown in Table 2 are tentatively assigned to the octahedral site.

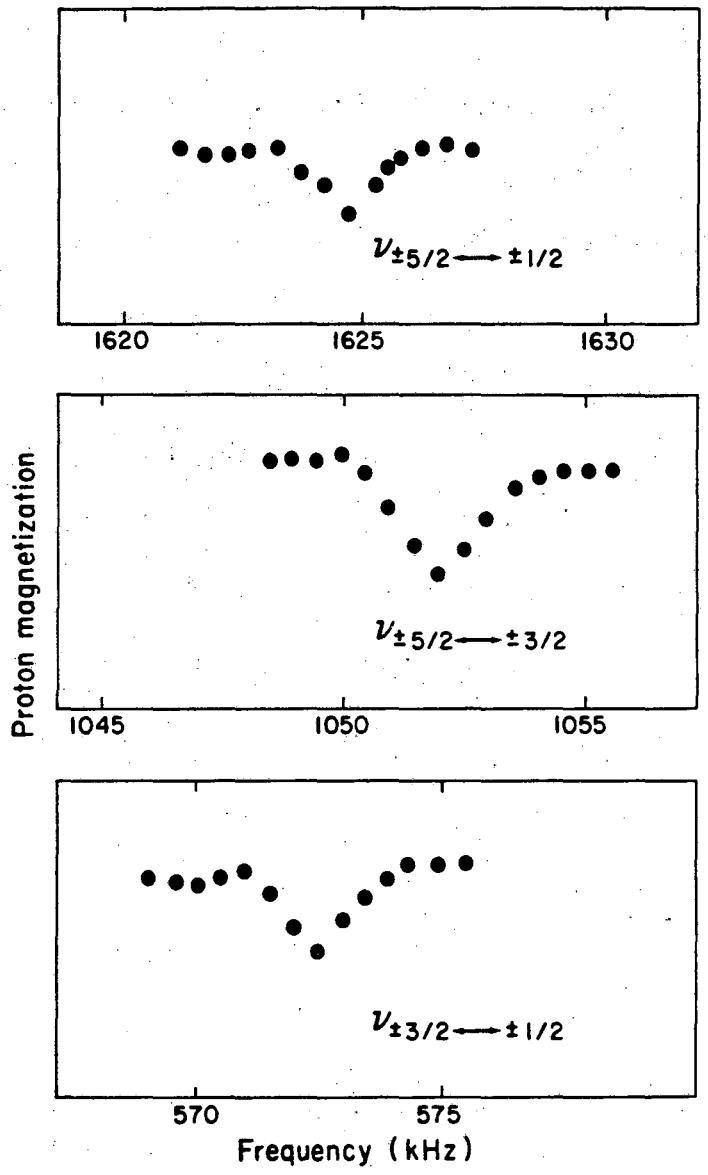

Figure 7. Al^{27} NQR lines in muscovite obtained by H^1-Al^{27} nuclear double resonance at room temperature.

It is not yet possible to draw many conclusions from this measurement. For comparison, the values for the Al in spodumene,[14] $LiAl(SiO_3)_2$, are e^2qQ= 2950 kHz, η = 0.94; other results can be found in the review by Ghose and Tsang.[24] Further work may show that it is possible to distinguish between tetrahedral and octrahedral aluminum on the basis of the NQR data. The narrow line widths seem indicative of a high degree of Al/Si positional order in this muscovite sample.

Further refinements are being made to the spectrometer to increase its sensitivity in order to search for the tetrahedral aluminum sites. These lines are expected to be weaker, and may lie at lower frequencies because of the high symmetry. The rather short value of the $T_{1\rho}(0)$ time (~ 400 msec) at room temperature indicates that higher sensitivity can be achieved at a lower temperature where T_1 may be longer. Nonetheless, the results to date are an encouraging first step in the laboratory analysis of alumino-silicate minerals.

2.3.2 Salt

Research to determine the induced quadrupolar coupling in stressed sodium chloride crystals was initiated with Dr. J. Ragle and Mr. J. Clymer of the Chemistry Department, University of Massachusetts, Amherst. Based on calculations in Ref. 1, an applied uniaxial stress of 100 atm should produce quadrupole energy levels of about 5 kHz. Since this value is very low, the best hope of success was to employ Na^{23}-$Cl^{35,37}$ double resonance techniques.

Accordingly, a special sample holder (Fig. 8) was designed by Mr. L. Hansen of the LBL Mechanical Engineering Department and constructed in LBL shops. This holder is capable of producing a uniaxial stress of 50-150 atm on a crystal of salt 0.5 inch in diameter by 1.0 inch long. The salt is held in

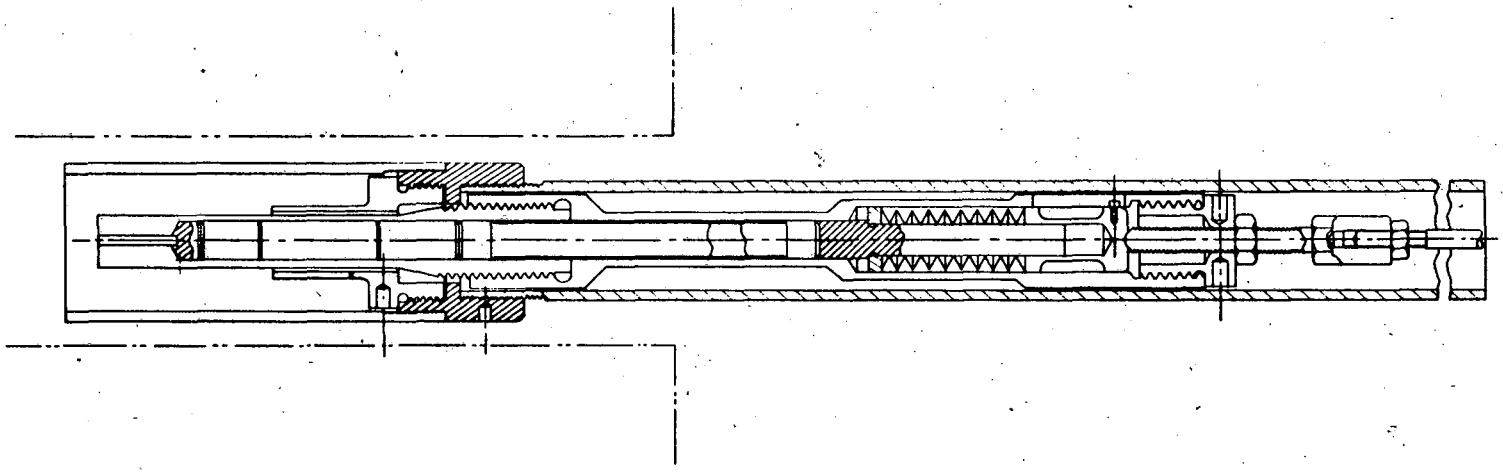

XBL 823-1964

Figure 8. Jig for stressing salt single crystals for nuclear magnetic NQR double resonance measurements. The overall dimensions are about 1.5 inches in diameter by 14 inches long. Stresses up to 150 atm are possible.

a bakelite tube in order to allow radio waves to penetrate and is constructed of nonmagnetic materials except for the steel Belleville springs which provide the pressure.

Single crystals of sodium chloride machined to size were obtained from the Harshaw Chemical Co. These were oriented with either the [111] axis or the [110] axis parallel to the cylinder. Pressure was applied to the crystal ends by machined ceramic anvils. Polycrystalline NaCl was also used.

There were two major questions to be answered by these studies: Whether the effects of applied stress were measurable on the sodium pure NMR signal in high field and whether the sodium natural dipolar linewidth would obscure attemps to observe the pressure-dependent chlorine pure quadrupolar absorption at zero field and at typical values of geologic stress. The experimental results are summarized in Table 3 and Figs. 9 to 20.

2.3.2.1 Sodium NMR Linewidth. When stressed, the cubic symmetry of sodium chloride is lifted, which means that the sodiums now experience a non-zero EFG and the resulting quadrupolar splitting is impressed on the Zeeman levels.[1] Thus, a uniaxial stress is expected to result in a broadening of the NMR line. This broadening in frequency space is equivalent to a shortening of the FID in the time domain.[10,11] In general, the linewidth $\Delta\omega$ is related to the spin-spin relaxation time T_2^* by

$$\Delta\omega = \frac{1}{T_2^*} \cdot \qquad [9]$$

At room temperature and at zero applied stress, T_2^* for Na^{23} in Harshaw [111]-oriented NaCl is about 105 μsec ($\Delta\omega \simeq 10$ kHz). At an applied stress of 150 atm, T_2^* shortens to about 50 μsec ($\Delta\omega \simeq 20$ kHz), i.e., a change by a factor of two. This value does not change measurably after 24 hours at stress, and

TABLE 3. Summary of experiments performed on salt.

Sample	Applied stress	Level crossing attempted	rf polarization (at zero field)
Polycrystalline, reagent grade	0 atm	No	--
	100 atm	No	--
	150 atm	No	--
[110] single crystal rod	0 atm	Yes	Parallel and perpendicular to stress
	100 atm	Yes	As above
	150 atm	Yes	As above
[111] single crystal rod	0 atm	Yes	As above
	100 atm	Yes	As above
	150 atm	Yes	As above
	150 atm to 0 atm short- and long-term relaxation		

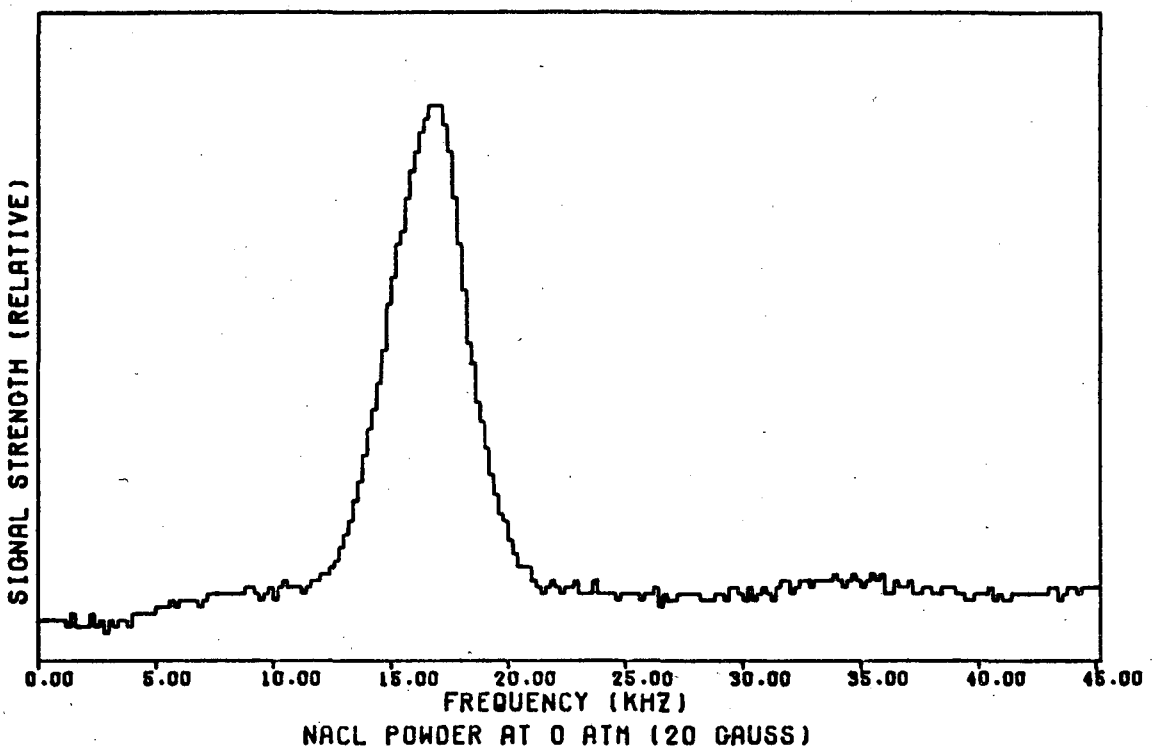

Figure 9. Low-field sodium NMR spectra at zero applied stress by adiabatic demagnetization double resonance spectroscopy. The sensitivity of detecting sodium by this method is many orders of magnitude greater than for direct observation at the same field. The applied static field is 20 gauss, and the spectrum represents a single data collection pass at ambient temperature (20°C) on a sample of approximately 3 grams of powdered reagent grade sodium chloride. Compare this spectrum with that in Fig.10 at 100 atm applied stress, and also with the zero-field spectra of Figs. 16 and 17. The small peak centered at 35 kHz is likely due to sodium $\Delta m = 2$ transitions which are forbidden at high field.

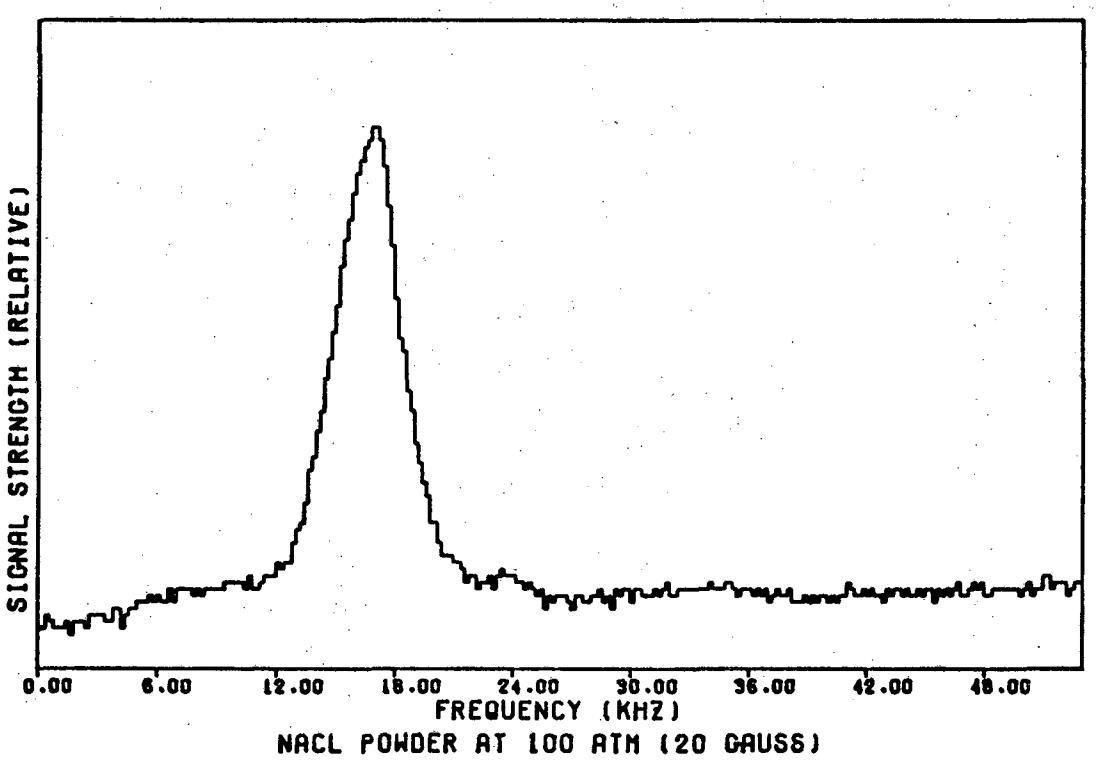

Figure 10. Low-field sodium NMR spectrum at 100 atm applied stress. The applied field is 20 gauss and the data were taken at ambient temperature. No broadening is evident due to sodium nuclear quadrupole coupling when data are taken in this fashion. Compare the spectra in Figs. 9 and 10 with the spectra in Fig. 11 obtained at high field by Fourier transform spectroscopy.

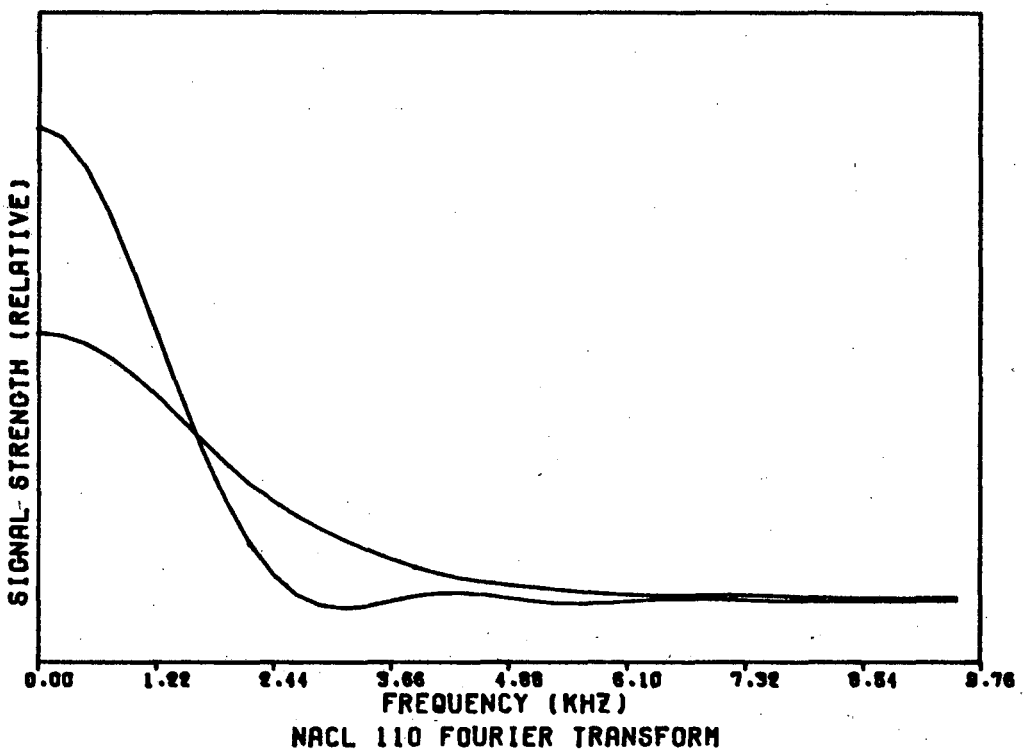

Figure 11. Fourier-transformed high field sodium NMR spectra for single crystal rods of Harshaw sodium chloride taken with the applied stress parallel to the [110] crystallographic axis. Half of each lineshape is shown. The narrower line corresponds to the applied stress; the broader line was taken at 100 atm stress. The slight beat note in the zero stress spectrum is due to apodization error in the FFT computation. Actually it is much less time consuming and error prone to utilize the time-domain sodium signals directly to measure pressure than to subject them first to Fourier transformation, since the Fourier transform requires an extrapolation to zero time, a data tabulation, and the Fourier transform operation, while the time domain measurement simply requires the measurement of a decay time.

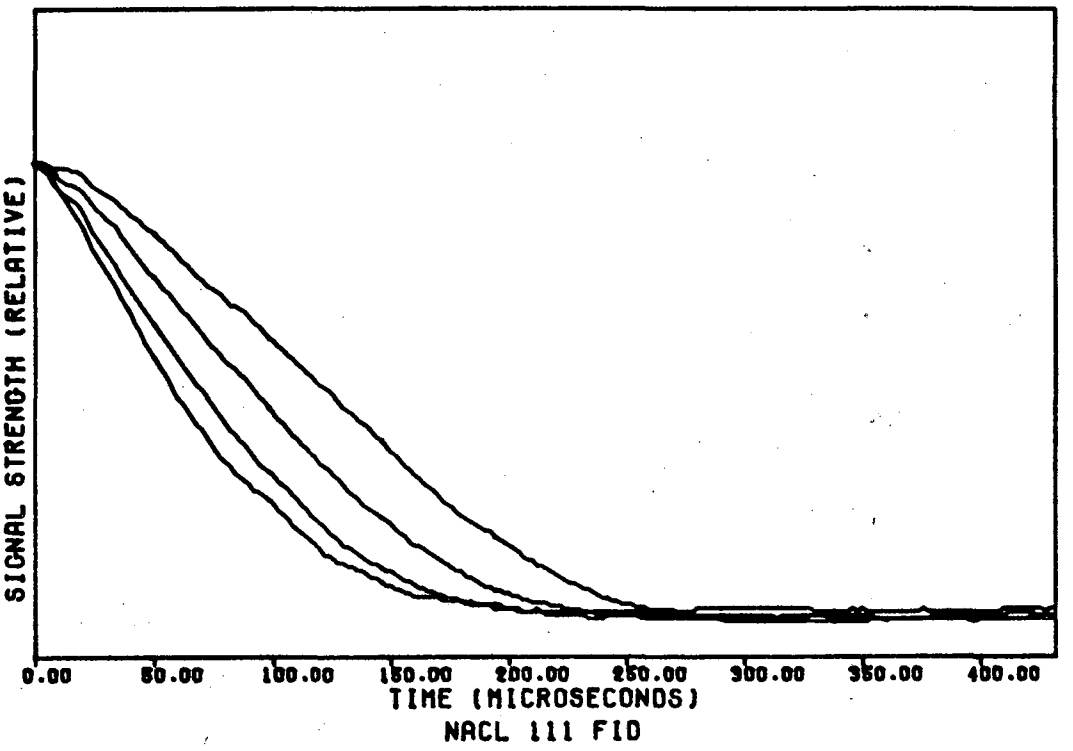

Figure 12. Sodium free induction signals in Harshaw single crystal rod, with stress applied along the crystallographic [111] direction. Applied stress values are, from top to bottom, 0 atm, 93.3 atm, 135.5 atm, and 151.8 atm.

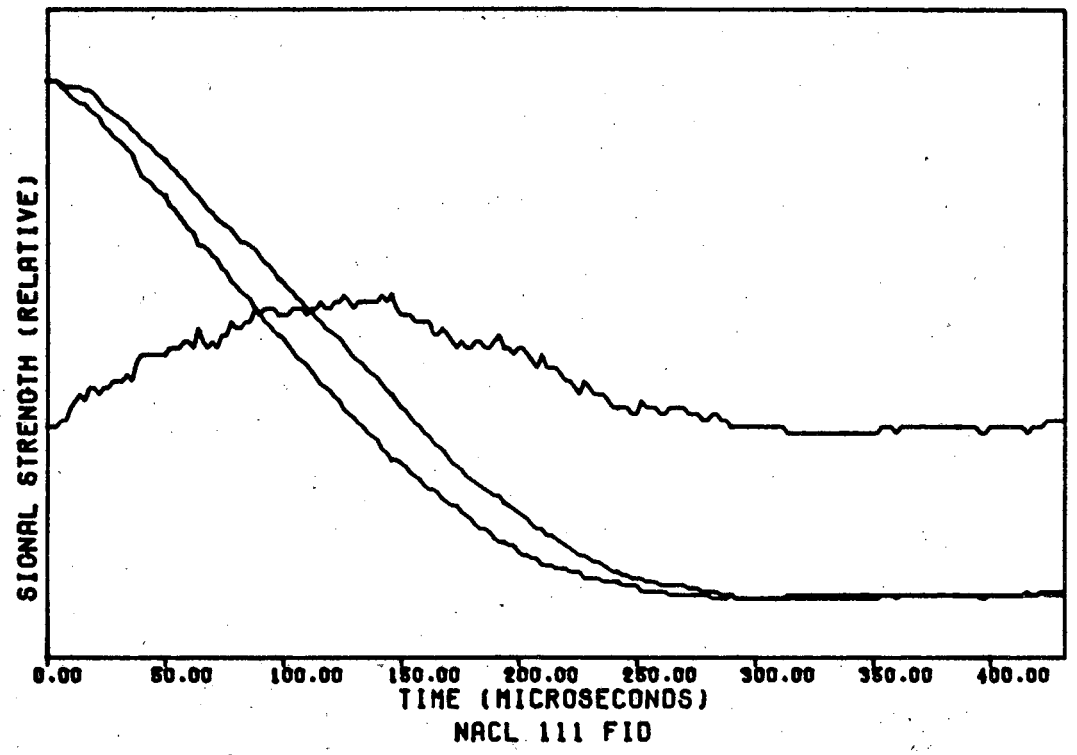

Figure 13. Sodium free induction signals in Harshaw single crystal rod, with stress = 0 atm (upper curve) and with stress cycled to 0 atm after several hours at 151.8 atm (lower curve). The difference between these curves, magnified twofold, is plotted in the center of the diagram.

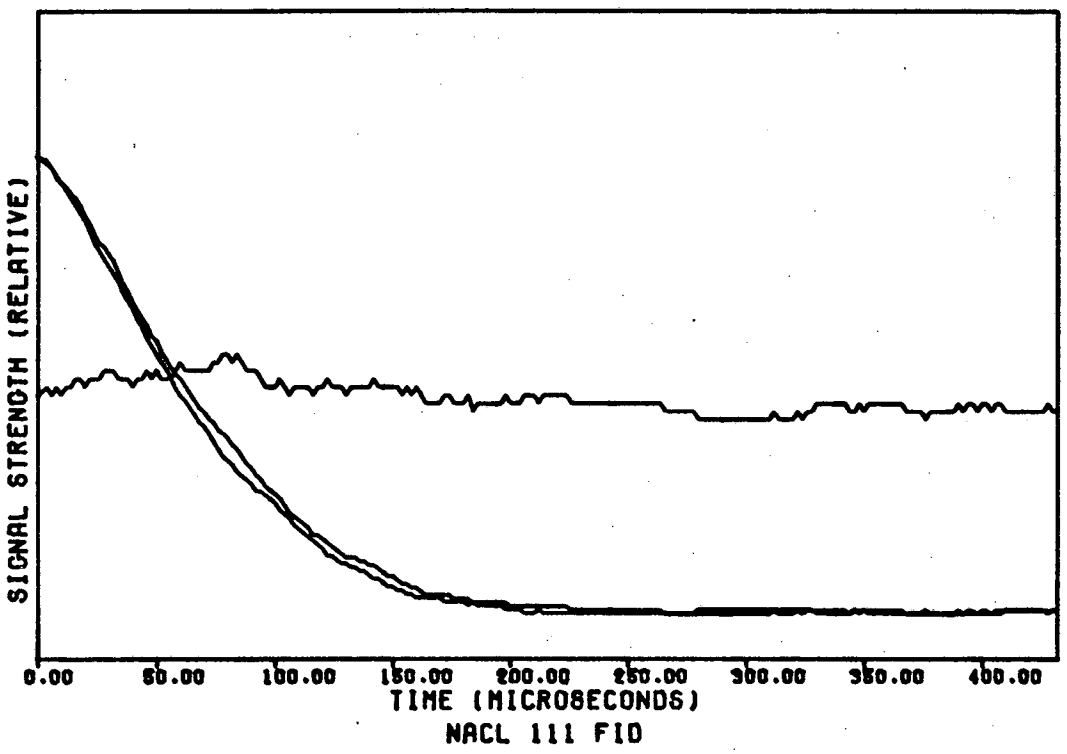

Figure 14. Sodium free induction signals in Harshaw single crystal rod, as in Fig. 13, except that the lower curve is immediately after attainment of 151.8 atm stress and the upper is taken after 3 hours at 151.8 atm.

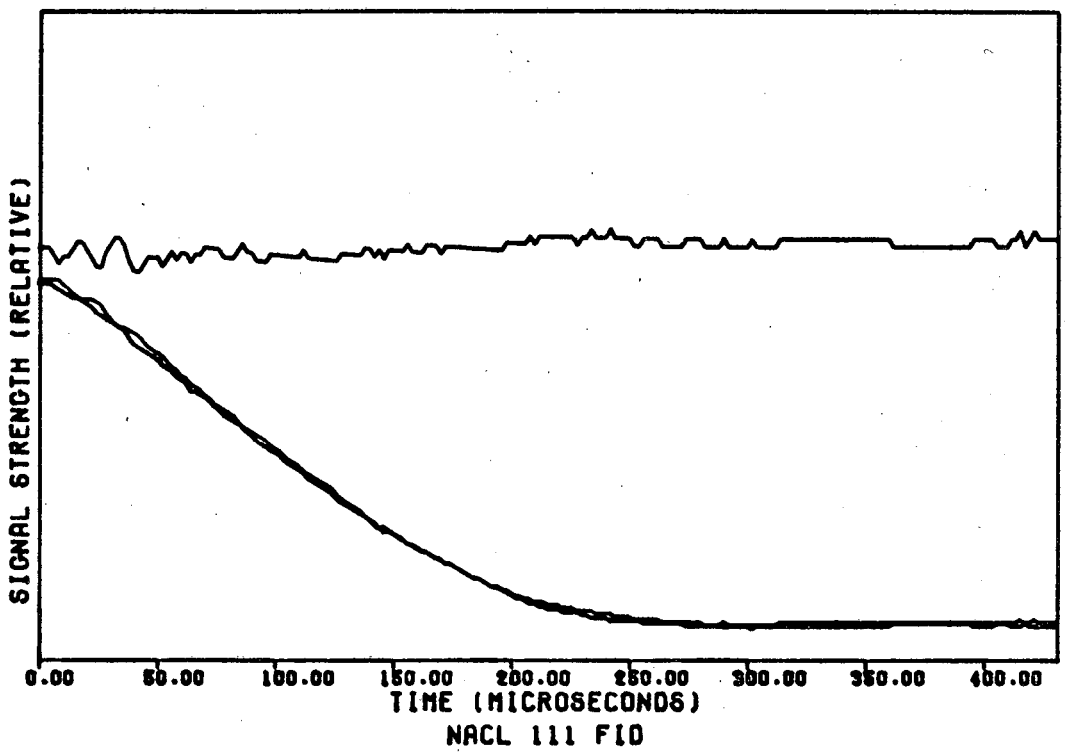

Figure 15. Sodium free induction signals in Harshaw crystal rod, as in Fig. 13, except that the two curves were taken 15 hours apart after destressing from 151.8 atm.

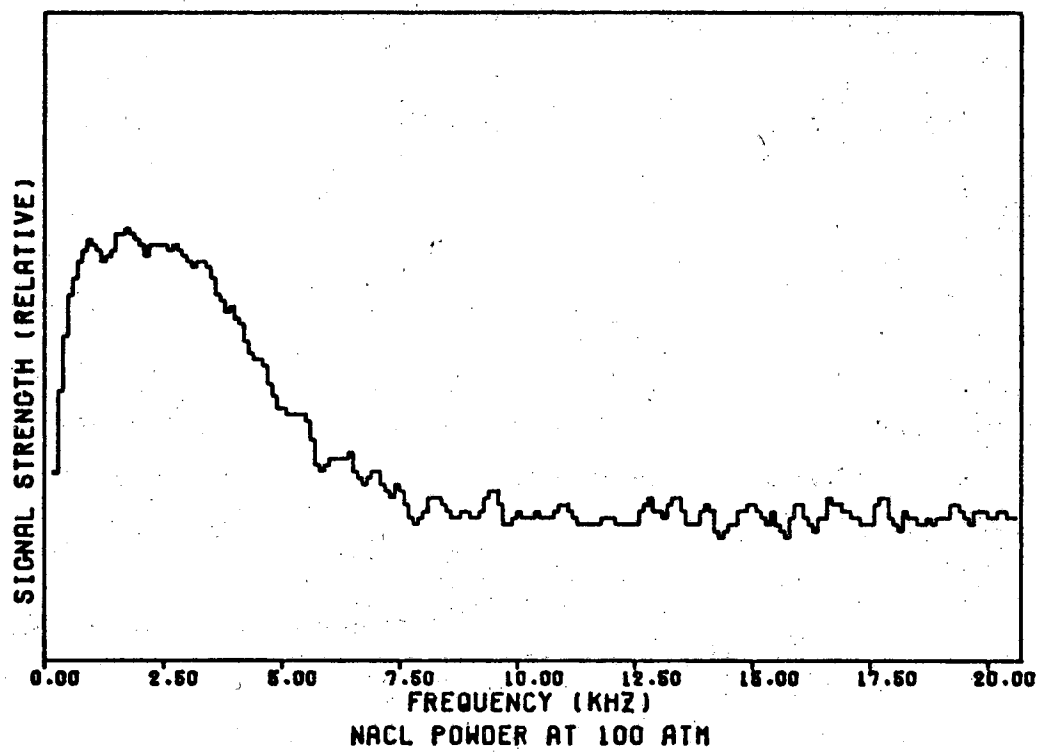

Figure 16. Double resonance spectrum of powdered NaCl at 100 atm stress.

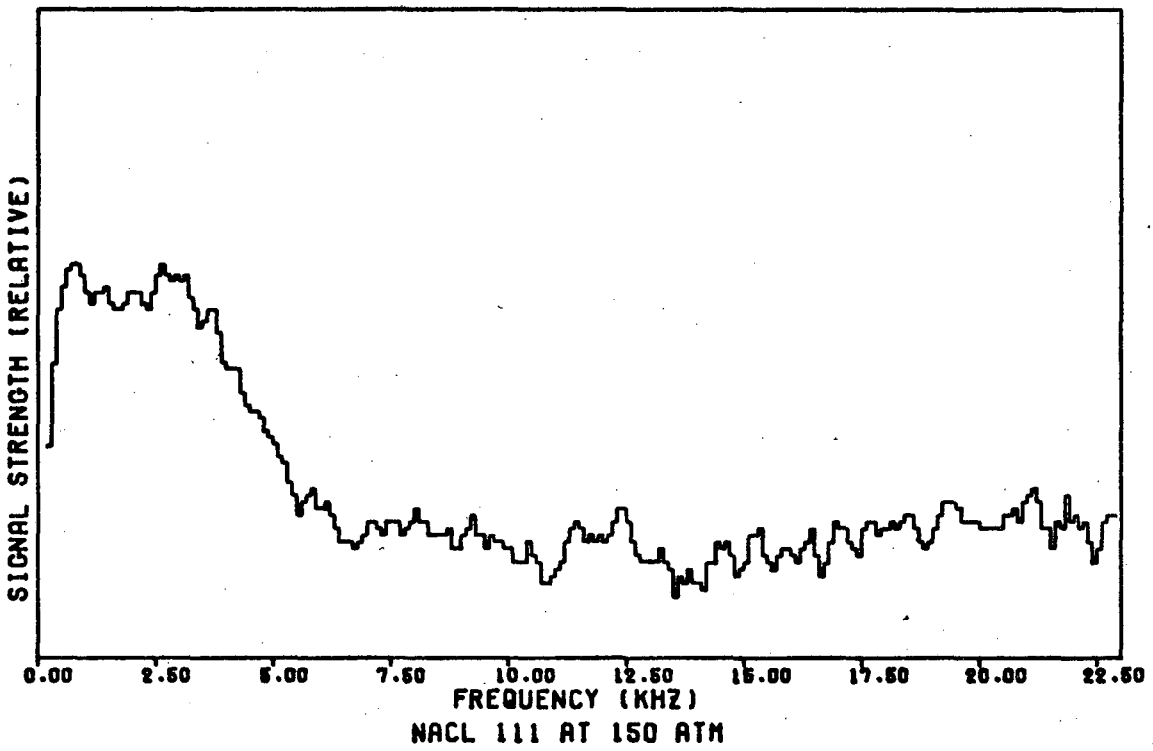

Figure 17. Double resonance spectrum of Harshaw single crystal rod, with an applied stress of 150 atm applied along the crystallographic [111] direction. Other spectra are dominated from 1 kHz to 5 kHz by sodium dipolar absorption and none of the spectra of this type show stress dependent features.

the sample recovers to within 1-2% of the original value within ten minutes after the stress is released. The remainder does not recover after 24 hours at the zero-stress level (see Figs. 14 and 15).

Over the entire range of applied pressure, the sodium high field NMR line shows no structure, either on the FID or on its Fourier transform. This means that the quadrupolar splittings remain unresolved even at 150 atm. Since these were predicted to lie in the 2-4 kHz range in Ref. 1, this is not surprising.

Results for [110]-oriented crystals were substantially similar. However, the effect of stress on polycrystalline samples was considerably smaller.

2.3.2.2 Level-Crossing Double Resonance Experiments. These experiments follow the experimental cycle described in Section 2.3.1.1: high field polarization of the sodiums, adiabatic demagnetization to zero field, irradiation, and adiabatic remagnetization to high field. This technique can provide very high sensitivity in the detection of the pure quadrupole spectra of species such as chlorine. However, the method fails when the dipolar absorption at low or zero field overlaps the spectra sought. Several such experiments were attempted for NaCl, but the dipolar absorption of the sodiums prevented observation of any stress-dependent features at low frequency (0-40 kHz) for any of the oriented or polycrystalline samples (Figs. 16 and 17).

2.3.2.3 Ultra-Low Field NMR Studies of Na. In attempting the level crossing experiments above, it was discovered that Na^{23} NMR lines can be observed in very low fields, 0.5 to 20 gauss. Since these lines were observed by monitoring the Na^{23} FID in high field in the normal course of cycling, it is apparent that this is a kind of "self double resonance." Such an experiment apparently has not been previously reported, but it holds

promise for studies of nuclear magnetic interactions in crystals at very low fields where the Zeeman Hamiltonian is dominated by the dipolar term. To the authors' knowledge, these experiments have demonstrated the lowest field spectra from solids ever reported. This work has also resulted in the detection of the $\Delta m=2$ transitions expected from the dipole term in the Hamiltonian.[6] Such transitions are rarely observed because of the strong $\Delta m = 1$ selection rule in high field experiments. Unfortunately, these low field spectra do not show any stress-dependent effects. Some experimental results are shown in Figs. 9 and 17 through 20.

2.3.2.4. Conclusions. A technique to measure stress in salt based on observation of the chlorine pure quadrupole absorption is not feasible owing to the strong dipolar absorption by the sodium nuclei at low field and low frequency. However, changes in the sodium spin-spin relaxation time seem to provide a practical avenue to the measurement of local stress. The threshold for such measurements may vary from 20-50 atm depending on whether the sample consists of large crystal grains or fine-grained polycrystalline material.

2.4 FURTHER CONSIDERATION OF THE EXPERIMENTAL DESIGN

The NQR spectrometer described in Section 2.1 remains the basic instrumental concept. It is easily adaptable to double resonance methods if these should be selected after further investigation. However, one alteration of the arrangement for producing a downhole magnetic field merits further consideration. In the original design[1], a simple solenoidal electromagnet was proposed to generate a field parallel to the borehole axis. A configuration using a pair of Helmholtz coils in opposition has been tested by Jackson and co-workers;[25-27] this scheme produces a homogeneous radial

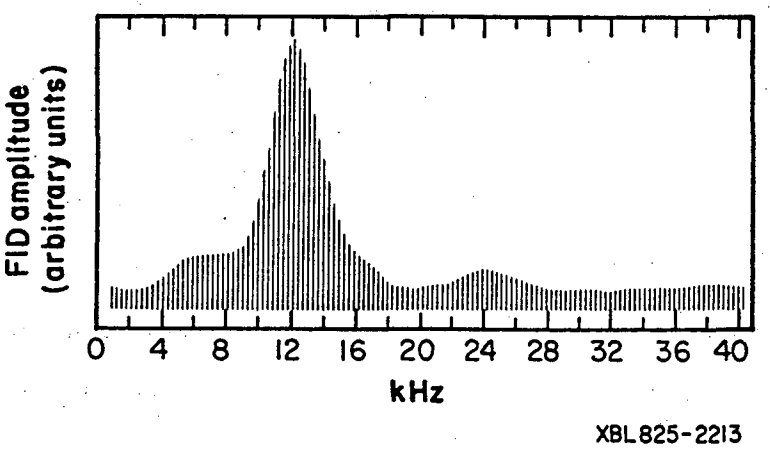

Figure 18. Sodium-free induction decay amplitude (vertical scale) versus irradiation frequency in the B-channel for NaCl powder at 0 stress. This represents Na "self double resonance"; the main peak is the Na NMR signal in a weak magnetic field (about 11 gauss). The small peak centered at 24 kHz is the $\Delta m = 2$ transition. The shoulder to the left of the main peak is not understood at present.

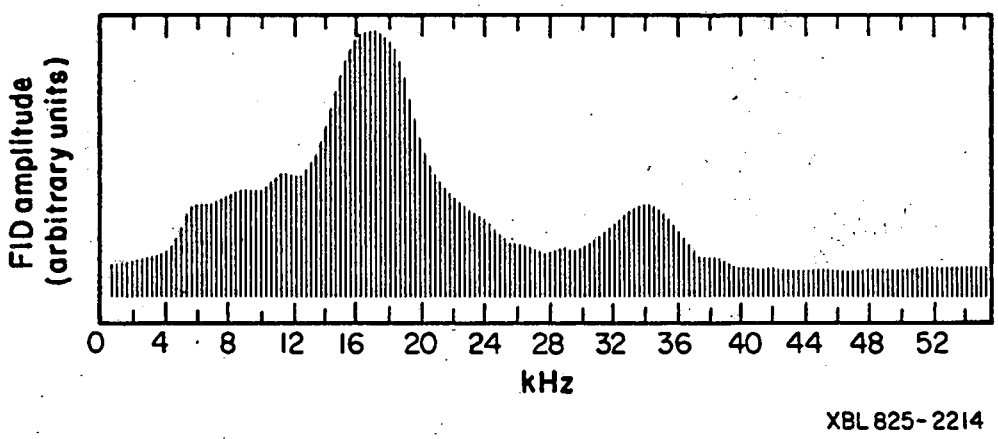

Figure 19. Same as Fig. 18 except that the NaCl powder is stressed at 100 atm and the magnetic field at the B-channel location has been increased to about 15 gauss. The $\Delta m = 2$ transition occurs at about 34 kHz.

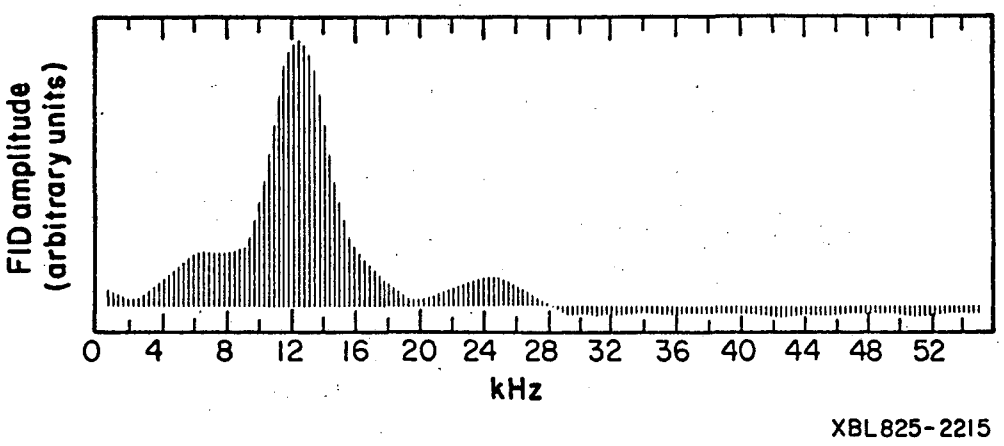

Figure 20. Sodium NMR signal in single crystal NaCl stressed at 150 atm parallel to [111] observed by "self double resonance." The B-channel field is about 11 gauss. The spectrum is almost identical to that obtained in an unstressed powder shown in Fig. 18.

magnetic field (and would require an rf coil whose solenoidal axis is parallel to the borehole). Experimental and computational work is necessary to decide which system is better.

It is recognized that the presence of paramagnetic species in the rock, chiefly Fe^{3+}, may shorten the Al^{27} spin-lattice relaxation time T_1. This could lead to line broadening and make double resonance experiments more difficult. Lack of experimental evidence to date makes further discussion speculative at this point.

Multiple sites for Al^{27} and Na^{23} may in some cases lead to an overlap of lineshapes. However, proton double resonance techniques, which preferentially detect nuclei physically close to the hydrogens, and double rf irradiation techniques, which can determine which transitions correspond to which site, can clarify and simplify the spectra. More sophisticated techniques such as two-dimensional spectroscopy are also available to improve resolution and to extract the essential data from the spectra. Moreover, little attention has been paid so far to the informational content contained in the values of the relaxation times; both theoretical and experimental work are required to maximize the data potential from these ground-breaking procedures.

3. CONCLUSIONS AND RECOMMENDATIONS

The work reported on the foregoing pages permits the following conclusions to be drawn.

- Work to date has enhanced the likelihood of final success in developing new instrumental techniques for the field measurement of stress in rocks containing alumino-silicate minerals.
- Severe problems exist in applying magnetic resonance methods to measure stress in salt and further efforts in this direction do not seem worthwhile.
- The successful observation of the quadrupole interaction in muscovite mica, an important constituent in many igneous and metamorphic rocks, indicates that common rock minerals will show observable resonance lines.
- Significant accomplishments have been achieved in understanding how the stress information is encoded in the lineshapes for polycrystalline material.
- The art of low frequency, pulsed NQR spectrometers has been advanced by the invention of a circuit for greatly reducing the after-pulse ringdown time.
- Mathematical considerations of the borehole perturbation indicate that NQR measurements can be used effectively to obtain values of the pre-existing state of stress.

It is obvious that considerable work remains. Based upon the experimental results with salt, we believe that salt is not favorable for further effort at this time, and we therefore recommend that the program concentrate

on the alumino-silicate minerals of granites and basalts. We thus recommend that future work follow the following program plan.

- Continue construction of the NQR spectrometer and complete the laboratory version.
- Carry out laboratory studies on well-characterized unstressed mineral species in polycrystalline form to detect the Al^{27} and Na^{23} NQR lines. Such minerals would include muscovite, vermiculite, biotite, diaspore, albite, microcline, epidote, and others. Compare different techniques for displaying the lines. The techniques of pure pulsed NQR, H^1-Al^{27} double resonance, Na^{23}-Al^{27} self double resonance, etc., would be evaluated. The effect of iron content on detectability, line width, etc., would also be investigated.
- Extend the work to actual rock samples, e.g., granite and basalt, to determine the sensitivity and resolution in a natural composite and real life situation. Some field tests could begin at this time. Concentrate on the alumino-silicate minerals of granites and basalts. (Salt does not seem favorable for further effort at this time.)
- Determine and calibrate the lineshape changes in the Al^{27} NQR spectra of single crystal and polycrystalline mineral samples as a function of hydrostatic and uniaxial stress in the laboratory. This would include studies of the effects of weak magnetic fields and rf orientation. Preliminary work could then be done on rock samples.

- Tabulate lineshapes and average frequencies as a function of stress for various materials and incorporate this information in computer programs which would relate a measured lineshape to the stresses which produced it.
- Finalize the design of a field version of the laboratory instrument based on the foregoing experiments. Both theoretical and experimental work will be required to optimize the construction details of the instrument for remote sampling.
- Develop computer programs to perform the full-scale reconstruction of the unperturbed stress tensor from borehole measurements in parallel with the above. Simulated stress input would include the NQR lineshape patterns measured in different directions and depths, the spatial resolution and rf homogeneity, the static dc magnetic field parameters, if needed, and the response curves of a cored rock sample to various laboratory stresses.
- Design, construct, and test the actual borehole spectrometer with associated computer software.
- Perform stress measurements in the field in well-characterized boreholes. This includes comparison of the NQR results with the stress measurements obtained using triaxial strain gauges, hydrofracture, and other conventional techniques.

REFERENCES

1. Schempp, E., Hirschfeld, T., and Klainer, S.M., The Measurement of In-Situ Stress in Salt and Rock Using NQR Techniques, Lawrence Berkeley Laboratory, Berkeley, California, LBL-11895 (1980).

2. Brown, R.J.C., J. Mol. Struct. 58, 85-88 (1980).

3. Armstrong, R.L., and Jeffrey, K.R., Can. J. Phys. 47, 309-313 (1969).

4. Slusher, R.E., Quadrupole Spectra of Rare Nuclei in Solids, Ph.D. Dissertation, Physics Department, University of California, Berkeley, 1966.

5. Edmonds, D.T., Phys. Reports C29, 233-290 (1977).

6. Slichter, C.P., Principles of Magnetic Resonance, Second Edition, Springer-Verlag, New York, 1978.

7. Fukushima, E., and Roeder, S.B.W., Experimental Pulse NMR, Addison-Wesley, Reading, Massachusetts, 1981.

8. Harding, J.C., Wade, D.A., Marino, R.A., Sauer, E.G., and Klainer, S.M., J. Magn. Reson. 36, 21-33 (1979).

9. Marino, R.A., Hunter College, New York, private communication.

10. Lowe, I.J., and Norberg, R.E., Phys. Rev. 107, 46-61 (1957).

11. Klainer, S.M., Hirschfeld, T.B., and Marino, R.A., "Fourier transform NQR spectroscopy," in Fourier, Hadamard, and Hilbert Transforms in Chemistry, A. Marshall, Ed., Plenum, New York, 1982.

12. Nye, J.F., Physical Properties of Crystals, Clarendon Press, Oxford, 1972.

13. Schempp, E., and Bray, P.J., "Nuclear quadrupole resonance spectroscopy," in Physical Chemistry, an Advanced Treatise, Vol. 4, H. Eyring, W. Jost, and D. Henderson, Eds., Academic Press, New York, 1970.

14. Harley, S.F., Williams, C.D., and Tipsword, R.F., J. Chem. Phys. 64, 4815-21 (1976).

15. Belitskiy, I.A., Shcherbakov, V.N., and Gabuda, S.P., Doklady Acad. Nauk SSSR 208, 154-157 (1973).

16. Jaeger, J.C., and Cook, N.G.W., Fundamentals of Rock Mechanics, Chapman and Hall, London (1976).

17. Jamison, D.B., and Cook, N.G.W., An Analysis of the Measured Values for the State of Stress in the Earth's Crust, Lawrence Berkeley Laboratory, Berkeley, California, LBL-7071 (1978).

18. Slusher, R.E., and Hahn, E.L., Phys. Rev. 166, 332-338 (1968).

19. Koo, J.C., Low Field Nuclear Quadrupole Resonance Spectroscopy, Ph.D Dissertation, Physics Department, University of California, Berkeley, 1970.

20. Edmonds, D.T., Hunt, M.J., Mackay, A.L., and Summers, C.P., "The high sensitivity detection of pure quadrupole resonance," in Advances in Quadrupole Resonance, Vol. I, Heyden and Son, Inc., London, 1974.

21. Feldes, H., and Livingston, R., Tables of Eigenvalues for Pure Quadrupole Spectra. Oak Ridge National Laboratory, Oak Ridge, Tennessee ORNL-1913 (1955).

22. Zvyagin, B.B., and Mishchenko, K.S., Kristallografia 5, 600 (1960).

23. Manguin, A.C., Compt. Rend. 185, 2888 (1972).

24. Ghose, S., and Tsang, T., Am. Mineral. 58, 748-755 (1973).

25. Cooper, R.K., and Jackson, J.A., J. Magn. Reson. 41, 400-405 (1980).

26. Burnett, L.J., and Jackson, J.A., J. Magn. Reson. 41, 406-410 (1980).

27. Jackson, J.A., Burnett, L.J., and Harmon, J.F., J. Magn. Reson. 41, 411-421 (1980).

APPENDIX

SPIN-3/2 STRESS-BROADENED POWDER LINESHAPES IN ALKALI HALIDES

In the absence of applied stress (and ignoring impurities or defects), nuclei in the cubic environment of an alkali halide crystal experience no electric field gradients and hence can have no NQR transitions. The application of uniaxial stress lowers the symmetry, creates field gradients at nuclear sites, and lifts the degeneracy of nuclear spin states.

These field gradients are described by the traceless second-rank electric field gradient (EFG) tensor $\underline{V}$ which can be diagonalized by

$$V = UV_dU\dagger, \qquad [1]$$

and characterized in terms of its three principal values: V_{xx}, V_{yy}, and V_{zz}. U is a three-dimensional rotation matrix. Assuming $|V_{zz}| \geq |V_{xx}| \geq |V_{yy}|$, we define

$$eq = |V_{zz}|,$$

and the asymmetry parameter, η, as

$$\eta = \frac{|V_{xx} - V_{yy}|}{eq} \qquad (0 \leq \eta \leq 1).$$

The electric field gradient tensor is related to the applied stress (also a second rank tensor) via the fourth-rank gradient-stress tensor $\underline{C}$:

$$V_{ij} = \sum_{kl} C_{ijkl}\ \sigma_{kl} \qquad [2a]$$

or in Voigt notation,

$$V_i = \sum_j C_{ij}\ \sigma_j, \qquad i=1,6;\ j=1,6. \qquad [2b]$$

For a general system, C_{ij} has 30 unique non-zero elements; fortunately, in a cubic system there are only two such elements, C_{11} and C_{44}. The nature of the EFG tensor depends on the orientation of the applied stress with respect to the crystal or crystallite of interest. We will choose a crystal coordinate system such that the $\underline{x}$, $\underline{y}$, and $\underline{z}$ axes lie along the [100], [010],

and [001] crystal directions, respectively. If we limit ourselves to uniaxial stress of magnitude σ_o and let θ and ϕ be the polar angles which describe the stress direction in the crystal frame, then the EFG tensor is given by the matrix

$$V = \sigma_o \begin{pmatrix} \frac{C_{11}}{2}(3\sin^2\theta\cos^2\phi - 1) & C_{44}\sin^2\theta\cos\phi\sin\phi & C_{44}\sin\theta\cos\theta\cos\phi \\ C_{44}\sin^2\theta\cos\phi\sin\phi & \frac{C_{11}}{2}(3\sin^2\theta\sin^2\phi - 1) & C_{44}\sin\theta\cos\theta\sin\phi \\ C_{44}\sin\theta\cos\theta\cos\phi & C_{44}\sin\theta\cos\theta\sin\phi & \frac{C_{11}}{2}(3\cos^2\theta - 1) \end{pmatrix} \quad [3]$$

A.1 CALCULATION OF FREQUENCIES AND AN APPROXIMATE LINE SHAPE IN NaCl

For spin-3/2 nuclei in zero magnetic field, the single NQR frequency ν is given by the following expression:

$$\nu_{NQR} = 1/2 \, \frac{eQ\,(eq)}{h} \, (1 + \eta^2/3)^{1/2} \, , \quad [4]$$

where Q is the nuclear quadrupole moment and $\underline{h}$ is Planck's constant. To calculate ν_{NQR} for a given relative orientation of stress and crystal, one could first calculate the elements of $\underline{V}$ as in Eq. 3, diagonalize $\underline{V}$, and then plug the resulting values of $\underline{eq}$ and $\underline{\eta}$ into Eq. 4. Alternately, it can be shown after sufficient manipulation that

$$\nu_{NQR} = 1/2 \, \frac{eQp}{h} \, \sigma_o, \quad [5]$$

where

$$p = \left[(4/3\ C_{44}^2 - 3C_{11}^2)(\sin^2\theta)(\sin^2\theta\ \cos^2\phi\ \sin^2\phi + \cos^2\theta) + C_{11}^2\right]^{1/2} \quad [6]$$

Note that the frequency is independent of the sign of C_{11} or C_{44}. For practical purposes, if C_{11} and C_{44} are expressed in units of 10^3 dyne$^{-1/2}$, Q in multiples of 10^{-24} cm^2, and σ_o in atm, then

$$\nu_{NQR} = 36.72\ Qp\sigma_o \quad (Hz). \quad [7]$$

The quantity $\underline{p}$ assumes simple forms when the stress is along characteristic crystal directions, as shown in Table A.1.

TABLE A.1. Variation in the parameter $\underline{p}$ with stress direction in cubic crystals.

Direction of stress	θ	ϕ	p*
[100]	90°	0°	$\lvert C_{11} \rvert$
[110]	90°	45°	$\left[1/3\ C_{44}^2 + 1/4\ C_{11}^2\right]^{1/2}$
[111]	54.7°	45°	$2/3\ \lvert C_{44} \rvert$

*The value of $\underline{p}$ will always lie between $\lvert C_{11} \rvert$ and $2/3\ \lvert C_{44} \rvert$.

If the alkali halide of interest is a powder, we must average over all crystal orientations with respect to the applied stress (or conversely, average all stress orientations relative to a single crystal). Equations 4-7 describe the frequencies expected in a powder spectrum. To completely specify the line shape, however, we must also know the NQR intensity for each orientation. As a first approximation, though, we can assume that intensity is independent of orientation. Equations 6 and 7 can then be used for generating a powder lineshape merely by calculating ν_{NQR} for a vast number of stress directions and adding 1.0 to the n^{th} point of the lineshape function whenever $\nu_n \leq \nu_{NQR} < \nu_{n+1}$.

For Cl^{35} in NaCl (for which $Q = -7.89 \times 10^{-2}$, $C_{11} = 8.0$, and $C_{44} = 30.8$, in units described above), the result is displayed in Fig. A-1 (a lineshape reminiscent of, but <u>not identical</u> to, an NMR chemical shielding powder pattern; see Fig. A-2). The three discontinuities in Fig. A-1 correspond to the application of stress along the three characteristic crystal directions. The frequencies are $\nu_{100} = 2.3$ kHz, $\nu_{110} = 5.3$ kHz, and $\nu_{111} = 5.9$ kHz.

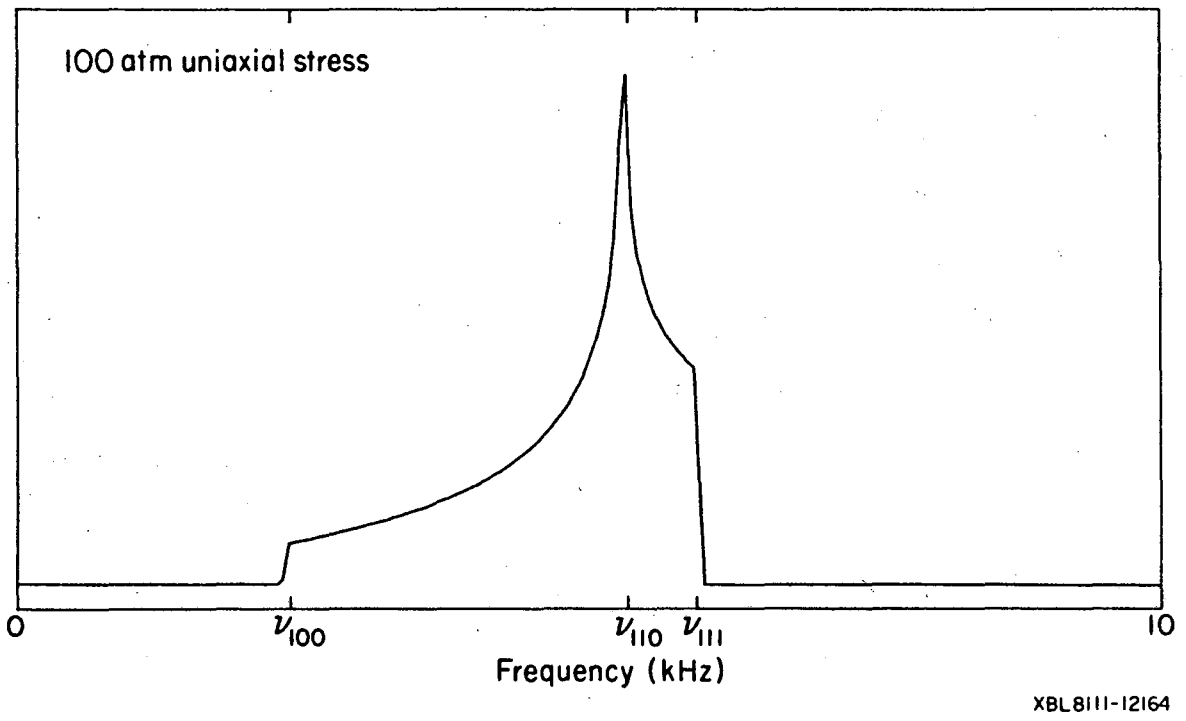

Figure A-1. Approximate NQR lineshape for a spin 3/2 nucleus in an alkali halide lattice assuming intensity is independent of orientation for a randomly oriented polycrystalline sample under uniaxial stress. ν_{100} is the frequency of crystallites whose [100] axis is parallel to the stress direction. The calculation used the values for Cl^{35} in NaCl.

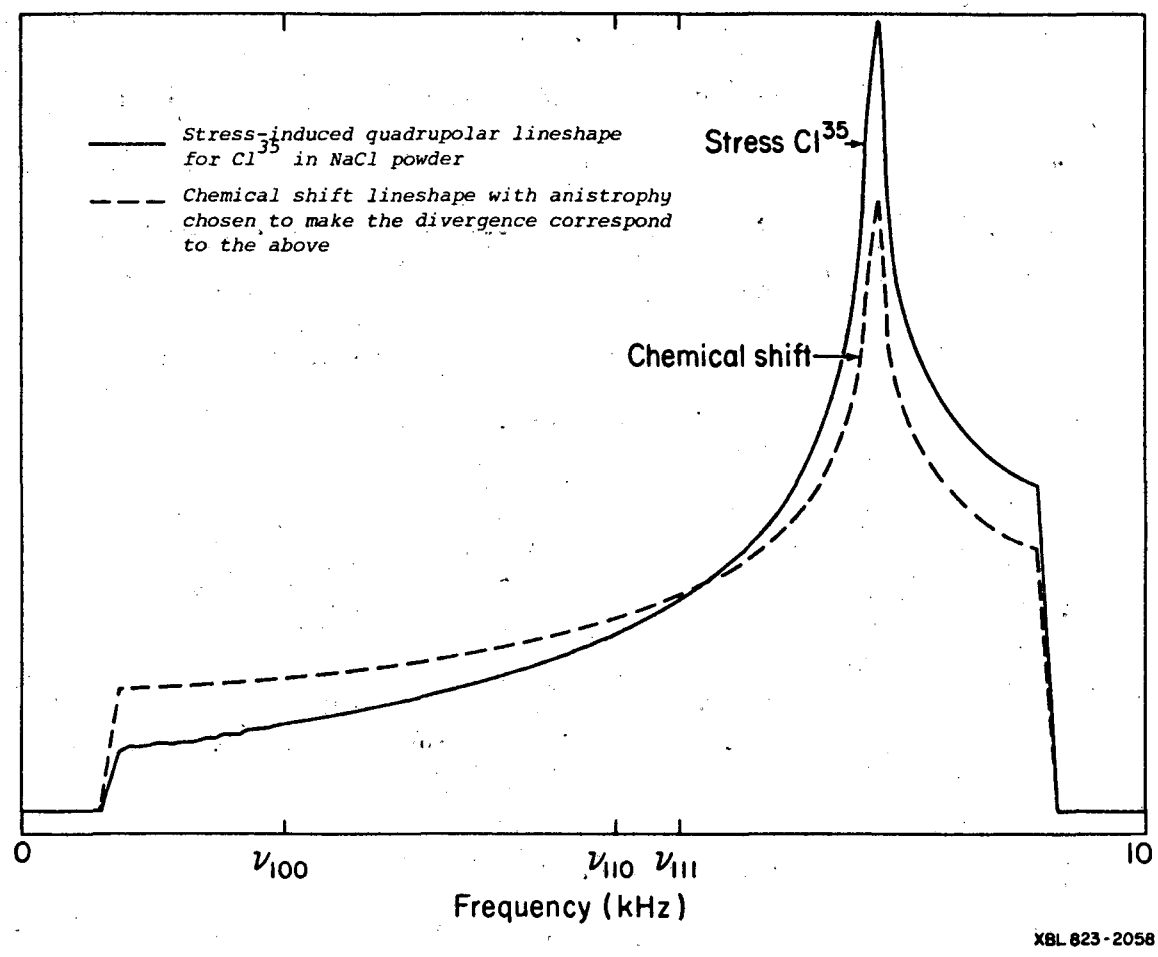

Figure A-2. Comparison of the stress-broadened NQR lineshape of Cl^{35} in polycrystalline NaCl under the equal intensity approximation with the chemical shift lineshape. The chemical shift anisotropy was chosen to make the divergences coincide to facilitate the comparison.

Note that, for simplicity, the effects of dipolar or defect broadening have been ignored. This is not to suggest that such broadening is expected to be trivial; only experimentation will tell how tenuous the link is between the spectra here and reality.

A.2 INTENSITIES: AN OUTLINE OF THE EXACT CALCULATION

When the actual intensity for each crystallite is included, the calculation becomes much more involved, and the orientation of the rf irradiation with respect to the applied stress must be specified. Two cases are considered: (1) the rf field parallel to the applied uniaxial stress, and (2) the rf field perpendicular to the stress. In either case, we assume that the stress defines the z-axis of the lab frame. The vectors describing the rf field are then

$$(1)\ h_z = \begin{pmatrix} 0 \\ 0 \\ 1 \end{pmatrix}, \qquad (2)\ h = \begin{pmatrix} \cos\alpha \\ \sin\alpha \\ 0 \end{pmatrix} = \cos\alpha \begin{pmatrix} 1 \\ 0 \\ 0 \end{pmatrix} + \sin\alpha \begin{pmatrix} 0 \\ 1 \\ 0 \end{pmatrix} = h_x\cos\alpha + h_y\sin\alpha \quad [8]$$

where α is the angle between the rf field orientation and some arbitrary lab x-axis. These vectors must be transformed first into the crystal coordinate system:

$$\begin{aligned} (1)\ h_z' &= R^\dagger h_z \qquad (2)\ h_x' = R^\dagger h_x \\ h_y' &= R^\dagger h_y \\ h_\perp' &= R^\dagger h_\perp \\ &= h_x'\cos\alpha + h_y'\sin\alpha \end{aligned} \quad [9]$$

$R^\dagger$ is a 3 x 3 transformation matrix:

$$R^\dagger = \begin{pmatrix} \cos\theta\cos\phi & -\sin\phi & \sin\theta\cos\phi \\ \cos\theta\sin\phi & \cos\phi & \sin\theta\sin\phi \\ -\sin\theta & 0 & \cos\theta \end{pmatrix}. \quad [10]$$

The next step is to transform the vectors again, this time into the principal axis system of the EFG tensor. Recalling that $V = UV_dU^\dagger$ or $V_d = U^\dagger VU$, we have

$$h''_z = U^\dagger R^\dagger h_z, \quad \text{and} \quad h''_x = U^\dagger R^\dagger h_x$$

$$h''_y = U^\dagger R^\dagger h_y \qquad [11]$$

$$h''_\perp = U^\dagger R^\dagger h_\perp$$

$$= h''_x \cos\alpha + h''_y \sin\alpha$$

The elements of $U^\dagger$ are obtained when $\underline{V}$ is diagonalized.

To proceed rigorously from this point, one also diagonalizes the NQR Hamiltonian:

$$H_{NQR} = \frac{e^2qQ}{12h}\left[3I_z^2 - I(I+1) + \frac{1}{2}\eta(I_+^2 + I_-^2)\right] \qquad [12a]$$

$$H_{NQR} = SES^\dagger \quad (E \text{ is diagonal}). \qquad [12b]$$

where $\underline{S}$ denotes the eigenvector matrix. (Note that $\underline{H}$ is a 4x4 matrix in spin space rather than a 3x3 matrix in real space.) The elements of h''_z or $h''_\perp$ are the coefficients of I_x, I_y, and I_z in the spin-product basis set defined with z-axis parallel to the z-axis of the EFG tensor. The NQR intensity is therefore proportional to

$$(1) \quad \text{Trace}\left\{[(S^\dagger)(h''_{z1}I_x + h''_{z2}I_y + h''_{z3}I_z)(S)]^2\right\}\ \delta(\nu-\nu_{NQR}) \qquad [13a]$$

or

$$(2) \quad \text{Trace}\left\{[(S^\dagger)(h''_{\perp 1}I_x + h''_{\perp 2}I_y + h''_{\perp 3}I_z)(S)]^2\right\}\ \delta(\nu-\nu_{NQR}), \qquad [13b]$$

where $\delta(\nu-\nu_{NQR})$ is unity when $\nu=\nu_{NQR}$ and zero otherwise.

Averaging over the angle α is appropriate in the second case since the sample is a powder. The second expression thus becomes

$$\frac{1}{2}\left[\text{Trace}\left\{[(S^{\dagger})(h''_{x1}\ I_x + h''_{x2}\ I_y + h''_{x3}\ I_z)(S)]^2\right\}\right.$$
$$\left. + \text{Trace}\left\{[(S^{\dagger})(h''_{y1}\ I_x + h''_{y2}\ I_y + h''_{y3}\ I_z)(S)]^2\right\}\right]\ \delta(\nu-\nu_{NQR}) \qquad [14]$$

The approach described above is used for the computer generation of stress-broadened NQR lineshapes with exact intensities (Figs. A-3 and A-4). To summarize, the procedure is as follows:

- Choose an rf field parallel or perpendicular to the applied stress.
- Choose a large number of stress orientations relative to a fixed crystal frame.

For each stress orientation,

- Use Eq. 3 to set up the EFG tensor $\underline{V}$.
- Diagonalize $\underline{V}$ to obtain $\underline{U}^{\dagger}$, $\underline{eq}$, and $\underline{\eta}$.
- Use either Eq. 4, or Eq. 6 and Eq. 7, to calculate ν_{NQR}.
- Use $\underline{eq}$ and $\underline{\eta}$ to set up a matrix for H_{NQR}.
- Diagonalize H_{NQR} to get the eigenvector matrix $\underline{S}$.
- Transform the rf vector(s) h_z or h_x, h_y into the EFG principal axis frame using Eq. 11.
- Use Eq. 13a or Eq. 14 to calculate the intensity.
- Add this intensity value to the n^{th} point of the simulated spectrum, where $\nu_n \leq \nu_{NQR} < \nu_{n+1}$.

A.3 RESULTS AND DISCUSSION

Basically, the intensity for a particular orientation of crystal and stress is greatest when the rf field is perpendicular to the z-axis of the EFG tensor and smallest (zero) when the rf field and the EFG z-axis are

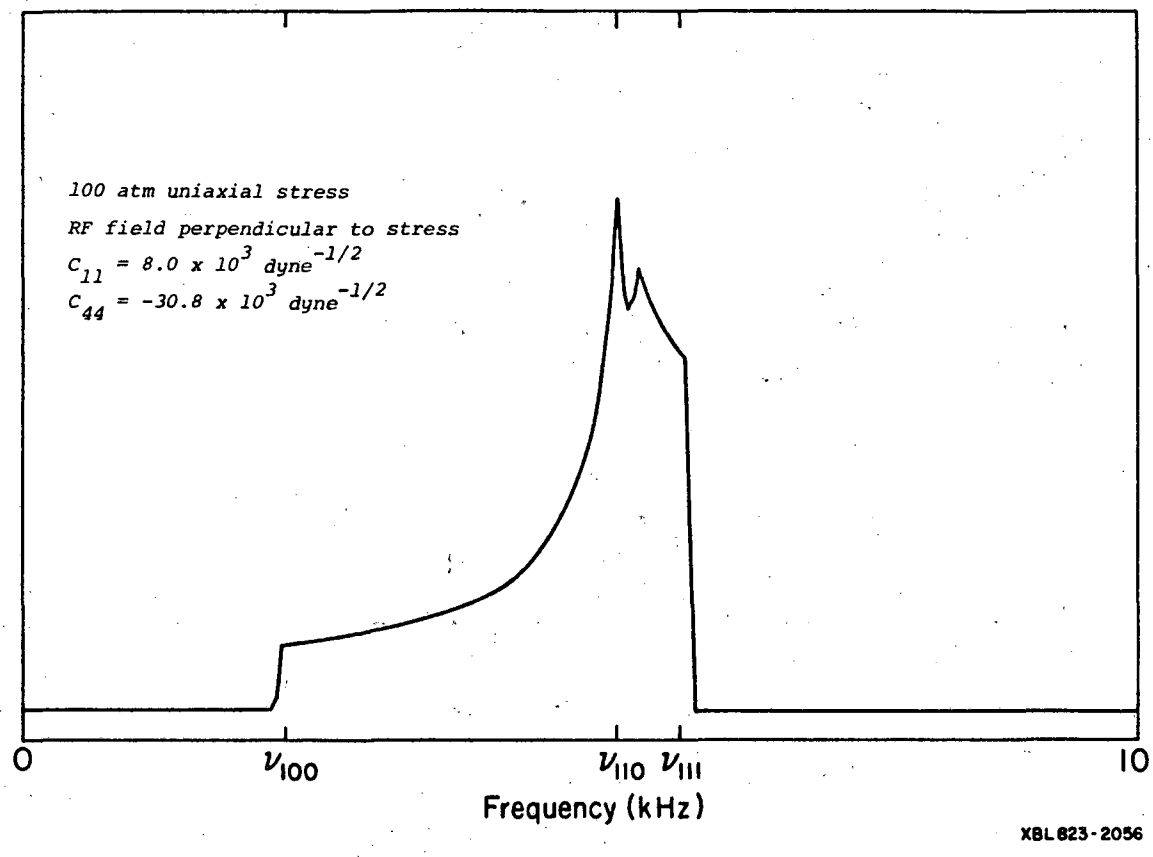

Figure A-3. Stress-broadened NQR lineshape of Cl^{35} in polycrystalline NaCl under 100 atm uniaxial stress corrected for variations in line intensity with differences in EFG orientation. Case I: The rf field is perpendicular to the stress direction. Compare Fig. A-1.

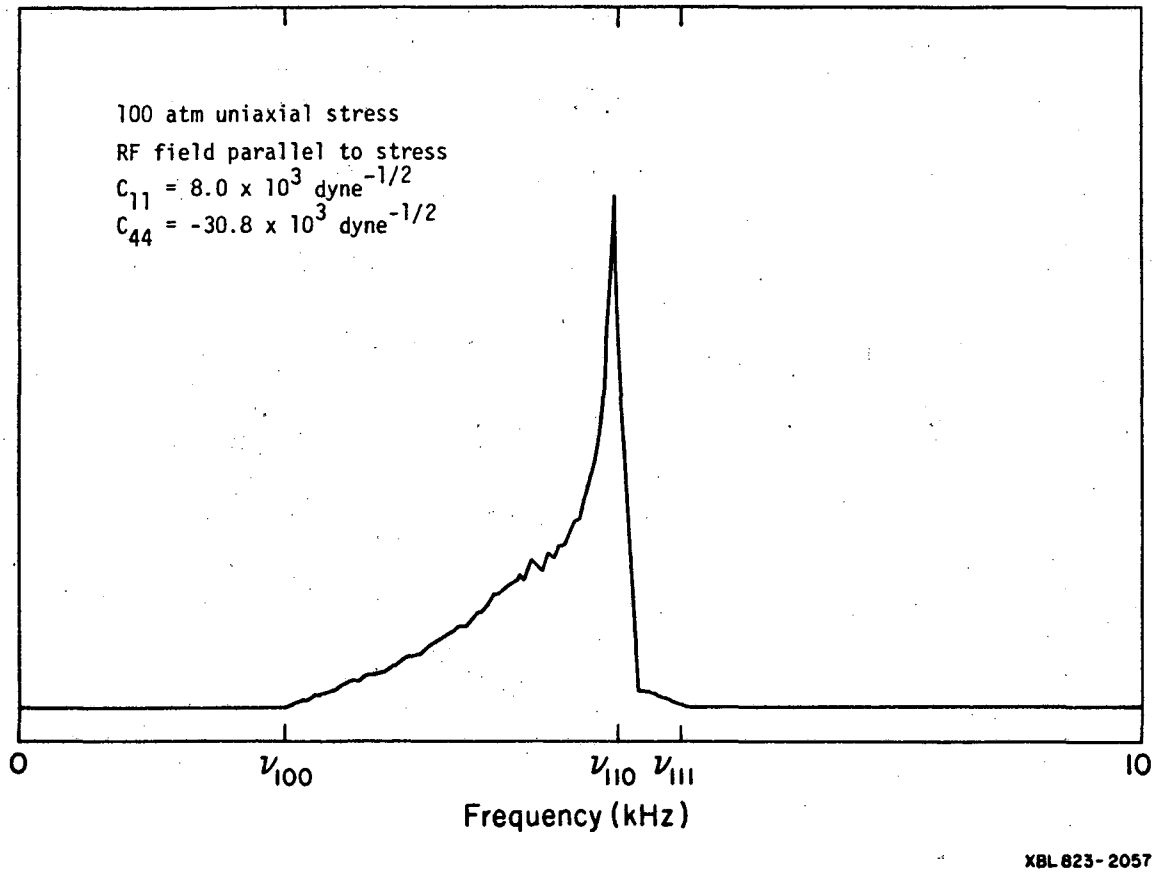

Figure A-4. Stress-broadened NQR lineshape of Cl^{35} in polycrystalline NaCl under 100 atm uniaxial stress corrected for intensity variations. Case II: The rf field is parallel to the stress direction. Compare Fig. A-3.

parallel. Experimentally, the rf irradiation can be parallel or perpendicular to the direction of applied stress. Thus the intensity for a given orientation can be estimated by knowing the angle between the stress direction and the resulting EFG z-axis. In short, if the rf is applied parallel to the stress, intensity is greatest when the EFG z-axis is perpendicular to the stress; if the rf is applied perpendicular to the stress, intensity is greatest when the EFG z-axis is parallel to the stress. These statements are most correct when η is small.

The matrix that transforms from the lab frame to the EFG principal axis system is $(U^{\dagger}R^{\dagger})$. If β is the angle between the stress direction and the EFG z-axis, then

$$\cos\beta = (U^{\dagger}R^{\dagger})_{3,3}. \qquad [15]$$

Examination of one matrix element thus yields the value of β.

It turns out that when stress is applied in either the [100] or [111] direction, the resulting EFG tensor is axially symmetric (η=0) and aligned parallel to the stress, no matter what the values of C_{11} and C_{44}. The rf field must, therefore, always be aligned perpendicular to the applied stress to detect the outer edges of the powder lineshape, ν_{100} and ν_{111} (cf. Figs. A-3 and A-4).

The case of stress along [110] is more interesting. For this orientation θ=90°, ϕ=45°,

$$R^{\dagger} = \begin{pmatrix} 0 & -1/\sqrt{2} & 1/\sqrt{2} \\ 0 & 1/\sqrt{2} & 1/\sqrt{2} \\ -1 & 0 & 0 \end{pmatrix}, \qquad [16]$$

and

$$V = \sigma_o \begin{pmatrix} \frac{1}{4} C_{11} & \frac{1}{2} C_{44} & 0 \\ \frac{1}{2} C_{44} & \frac{1}{4} C_{11} & 0 \\ 0 & 0 & -\frac{1}{2} C_{11} \end{pmatrix}. \qquad [17]$$

Diagonalizing $\underline{V}$, one obtains $V = UV_dU^\dagger$ in the form:

$$V = \sigma_o \begin{pmatrix} 1/\sqrt{2} & -1/\sqrt{2} & 0 \\ 1/\sqrt{2} & 1/\sqrt{2} & 0 \\ 0 & 0 & 1 \end{pmatrix} \begin{pmatrix} \frac{1}{4} C_{11} + \frac{1}{2} C_{44} & 0 & 0 \\ 0 & \frac{1}{4} C_{11} - \frac{1}{2} C_{44} & 0 \\ 0 & 0 & -\frac{1}{2} C_{11} \end{pmatrix} \begin{pmatrix} 1/\sqrt{2} & 1/\sqrt{2} & 0 \\ -1/\sqrt{2} & 1/\sqrt{2} & 0 \\ 0 & 0 & 1 \end{pmatrix} \qquad [18]$$

We must now determine which diagonal element of $\underline{V}_d$ has the greatest magnitude and hence is V_{zz}. Obviously this depends on the values of C_{11} and C_{44}. We can say nothing about the absolute sign of these quantities--only the relative sign. We will, therefore, assume that C_{11} is always positive.

For case 1,

$$C_{44} > \frac{1}{2} C_{11}$$

$$V_{zz} = \left| \frac{C_{11}}{4} + \frac{C_{44}}{2} \right|. \qquad [19]$$

The row of $U^\dagger$ corresponding to V_{zz} (the bottom row after appropriate rearrangement) is $(1/\sqrt{2} \quad 1/\sqrt{2} \quad 0)$. $(U^\dagger R^\dagger)_{3,3} = 1$, so the EFG z-axis is <u>parallel</u> to the stress.

For case 2,

$$-\frac{1}{2}C_{11} < C_{44} < \frac{1}{2}C_{11}$$

$$V_{zz} = \left|\frac{-C_{11}}{2}\right|. \qquad [20]$$

The row of $U^{\dagger}$ corresponding to V_{zz} is (0 0 1). $(U^{\dagger}R^{\dagger})_{3,3} = 0$, so the EFG z-axis is perpendicular to the stress.

For case 3,

$$C_{44} < -\frac{1}{2}C_{11}$$

$$V_{zz} = \left|\frac{C_{11}}{4} - \frac{C_{44}}{2}\right|. \qquad [21]$$

The row of $U^{\dagger}$ corresponding to V_{zz} is $(-1/\sqrt{2} \quad 1/\sqrt{2} \quad 0)$. $(U^{\dagger}R^{\dagger})_{3,3} = 0$, so the EFG z-axis is perpendicular to the stress.

Thus, when $C_{44} > \frac{1}{2}C_{11}$, the EFG z-axis is parallel to the applied stress for all three "special" crystal orientations: [100], [110], and [111]. Furthermore, when $C_{11} = 8.0$ and $C_{44} = 30.8$ (gradient-stress values for Cl in NaCl), the angle between the EFG z-axis and the stress never gets larger than approximately 14° at any orientation. As a result, the lineshape for the rf field aligned perpendicular to the stress is nearly identical to the first-approximation lineshape in Fig. A-1. If the rf field were aligned parallel to the applied stress, very little signal would result!

In comparison, when $C_{44} < \frac{1}{2}C_{11}$, the spectrum obtained with the rf field perpendicular to the stress will display the edges of the powder pattern (stress along [100] and [111]), but will be reduced in intensity near ν_{110}. Arranging the rf field parallel to the stress yields a narrower lineshape (no intensity at ν_{100} or ν_{111}) with a peak at ν_{110}. This behavior

is illustrated in Figs. A-3 and A-4. For these "pseudo-NaCl" spectra, only the sign of the chlorine C_{44} was changed. Hence, the frequency range covered is the same as in Fig. A-1 but the lineshapes are different. (Note that for aesthetic reasons, spectra in Figs. A-3 and A-4 are drawn to the same height; if plotted on the same scale, the A-4 spectrum would be slightly higher than the A-3 spectrum, and roughly half the height of the A-1 spectrum.)

A.4 COMPARISON OF NaBr WITH NaCl

For chlorine in NaCl, Kanert and Mehring[1] report that C_{11} and C_{44} do in fact have the same sign. Fig. A-1 is thus expected to be the correct Cl^{35} lineshape at 100 atm stress (again ignoring other sources of broadening). The frequency for Cl, unfortunately, is too low for successful detection with existing systems, but Br NQR frequencies are typically tenfold higher so it seems possible to verify these calculations empirically using NaBr. A comparison of the two compounds is shown in Table A.2.

TABLE A.2. Comparison of the quadrupolar stress parameters in NaCl and NaBr.

	$\lvert Q \rvert$ (10^{-24} cm^2)	C^*_{11}	C^*_{44}	Relative sign of C_{11} and C_{44}*
Cl^{35} in NaCl	7.89×10^{-2}	8.0	30.8	Same
Br^{79} in NaBr	0.33	--	68 or 130	Different
	(Factor of 4 difference)		(Factor of 2 or factor of 4 difference)	

*Values from Kanert and Mehring, op. cit.

[1]Kanert, O., and Mehring, M., "Static quadrupole effects in disordered cubic solids," in NMR Basic Principles and Progress, Vol. 3, p.34, Diehl, P., Fluck, E., and Kosfield, R., Eds., Springer-Verlag, New York, 1971.

The high-frequency edge (ν_{111}) of the stress-broadened powder lineshape of Br^{79} in NaBr is thus expected to fall between 8 and 16 times the comparable Cl^{35} in NaCl value, namely, between 47 and 94 kHz at 100 atm stress. The low-frequency edge (ν_{100}) for Br^{79} in NaBr can only be guessed, since C_{11} was not reported. If the ratio $|\frac{C_{44}}{C_{11}}|$ is the same for both species, then ν_{100} in Br^{79} would be expected in the range of 18 to 37 kHz at 100 atm stress. Since C_{44} and C_{11} have opposite signs for Br^{79} in NaBr, lineshapes would be expected to resemble Fig. A-3 or A-4 (depending on the rf alignment), but with frequencies increased by a factor of 8 to 16.

The spectrum of Br^{81} in NaBr would, of course, be similar, with all frequencies scaled down by a factor of $\frac{Q_{Br^{81}}}{Q_{Br^{79}}} = \frac{0.28}{0.33} \simeq 0.84$. At 100 atm stress, ν_{100} would be 15-30 kHz and ν_{111} would be 40-80 kHz. There certainly would be considerable overlap of Br^{79} and Br^{81} lineshapes if both were present in the same experimental spectrum.

TECHNICAL INFORMATION DEPARTMENT
LAWRENCE BERKELEY LABORATORY
UNIVERSITY OF CALIFORNIA
BERKELEY, CALIFORNIA 94720